



DESY SUMMER STUDENT PROGRAMME 2012

GISAXS Simulation of Polystyrene GLAD Thin Films

Chuvashova Irina

Lomonosov Moscow State University, Russian Federation

6th September 2012

Supervisor:

Dr. Stephan V. Roth

Abstract

This report describes work that has been done under supervision of Stephan Roth during the Summer Students Program 2012 at DESY. The research was concerned with the simulation of the process of growing polystyrene (PS) coated silicon (Si) substrate with nanoparticles of gold (Au) using GLAD technique and GISAXS analysis. The aim was to simulate the first and the last stages of the process with FitGISAXS. The results were compared with the experimental data. It is found what parameters make the greatest contribution to the process in simulation and found values of these parameters.

Contents

Introduction	3
Theory	4
Simulations.....	8
What is FitGISAXS?	8
Experimental Data	9
Layer geometry: what to choose?	12
Size distribution models.....	15
Other parameters.....	19
Structure factor	19
Form factor	23
Distance	34
Including SiO ₂ layer	41
Conclusions	44
References	45
Acknowledgments.....	46
Comments	47

Introduction

Small angle x-ray scattering (SAXS) is a very well-established measurement tool that has been around for about 70 years. It is "special" in terms of the distinction between SAXS and regular wide-angle x-ray scattering by virtue of the location of the scattering of interest. This is typically at small angles in the vicinity of the primary beam and extending to less than 2 degrees for standard wavelengths. The scattering features at these angles correspond to structures ranging from tens to thousands of angstroms.

Grazing incidence small-angle X-ray scattering (GISAXS) emerged to a versatile and frequently used analysis technique in the field of micro- and nanostructured thin films and surfaces. Among the various methods available to produce nanostructured thin films a very versatile procedure is the use of glancing angle physical vapor deposition (GLAD). This method produces porous thin films formed by columns tilted by a certain angle with respect to the substrate. One of the advantages of GISAXS is the ability to provide averaged statistical information over the entire illumination sampled area, as well as the ability to access buried structures located well below the surface that are not accessible to local probe techniques like scanning electron microscopy (SEM) or atomic force microscopy (AFM). The GISAXS technique is a powerful tool to describe the nanostructure of GLAD thin films.

Theory

Within the last years, grazing incidence small-angle X-ray scattering (GISAXS) emerged to a versatile and frequently used analysis technique in the field of micro and nano-structured thin films and surfaces. GISAXS is used for the characterization of micro- and nano-scale density correlations and shape analysis of objects at surfaces or at buried interfaces for various classes of materials such as ceramics, metals, semiconductors, polymers, biopolymers, and soft matter. As a result, GISAXS provides an excellent complement to more conventional nano-scale structural probes such as atomic force microscopy (AFM) and transmission electron microscopy (TEM). Whereas both are operated in real space, GISAXS as an advanced scattering technique gives results in reciprocal space. In contrast to standard small-angle X-ray scattering (SAXS) GISAXS is performed in reflection geometry. Thus GISAXS has somewhat similarities with SAXS and can be understood as a SAXS experiment performed in another scattering geometry (replacing transmission by reflection geometry). Alternatively, GISAXS can be envisaged as the extension of grazing incidence diffraction (GID) to small scattering angles or as a sort of diffuse reflectivity. Consequently, three different X-ray communities, SAXS, GID, and diffuse reflectivity are converging through GISAXS [1].

High-resolution GISAXS, now frequently named grazing incidence ultra-small angle X-ray scattering (GIUSAXS), was developed by Peter Müller-Buschbaum. As in transmission geometry (SAXS to USAXS), the regime of accessible lateral lengths was increased and structures above 10 micrometers were detected [2]. Therefore in combination with GISAXS and GIUSAXS an extremely large regime of lateral structures can be probed, starting on the nanometer level and ending with several micrometers. Anomalous small-angle X-ray scattering (ASAXS), using tuneable X-ray energies near, but below, X-ray absorption edges of the elements comprising in the investigated sample, in reflection geometry are meanwhile performed as well. Thus element-specific information, composition, and density fluctuation can be obtained for micro- and nano-structures in thin films and at interfaces.

Today key features of GISAXS are the ability to access

- an averaged statistical significant information over all the illuminated sample area (which is for common beam sizes in the range of square centimeters);
- buried structures, which are located well below the surface and thus are inaccessible to local probe techniques such as AFM;
- a depth-dependent structural information using different incident angles;

- structures in any kind of environments ranging from ultra-high vacuum to gas atmospheres and liquids;
- kinetic studies performed as function of external parameters such as temperature, gas pressure, pH, or ion concentration;
- structures in a non-invasive and non-destructive way.

The principle of GISAXS is sketched in Fig. 1a. The sample surface defines the (x,y) -plane with the x -axis oriented along the X-ray beam direction and thus the y -axis being perpendicular to the scattering plane given through the incident angle α_i and the exit angle α_f . The z -axis is representing the surface normal and as a consequence, the scattering plane is the (x, z) -plane (see Fig. 1b). Specular scattering fulfills the condition $\alpha_i = \alpha_f$, whereas off-specular or diffuse scattering satisfies $\alpha_i \neq \alpha_f$.

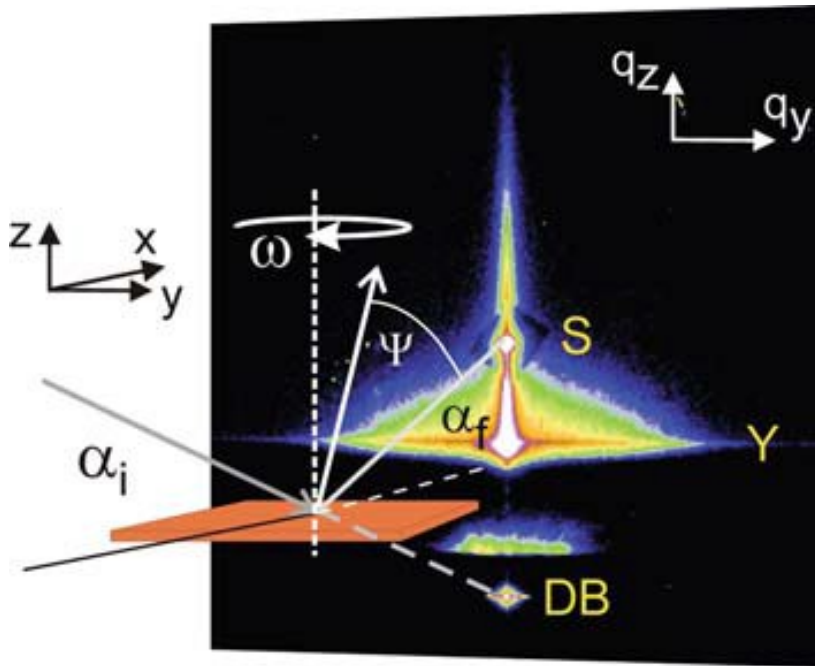


Fig. 1a. Schematic picture of the GISAXS scattering geometry. The sample is positioned with respect to the spatial coordinates x , y , and z as well as by its azimuthal orientation ω . The incident angle is denoted α_i , the exit angle α_f , and the out-of-plane angle ψ . The color coding visualizes differences in the scattered intensity on the two-dimensional detector. Main characteristic features are the specular peak (denoted S), the Yoneda peak (denoted Y), and the direct beam (denoted DB)

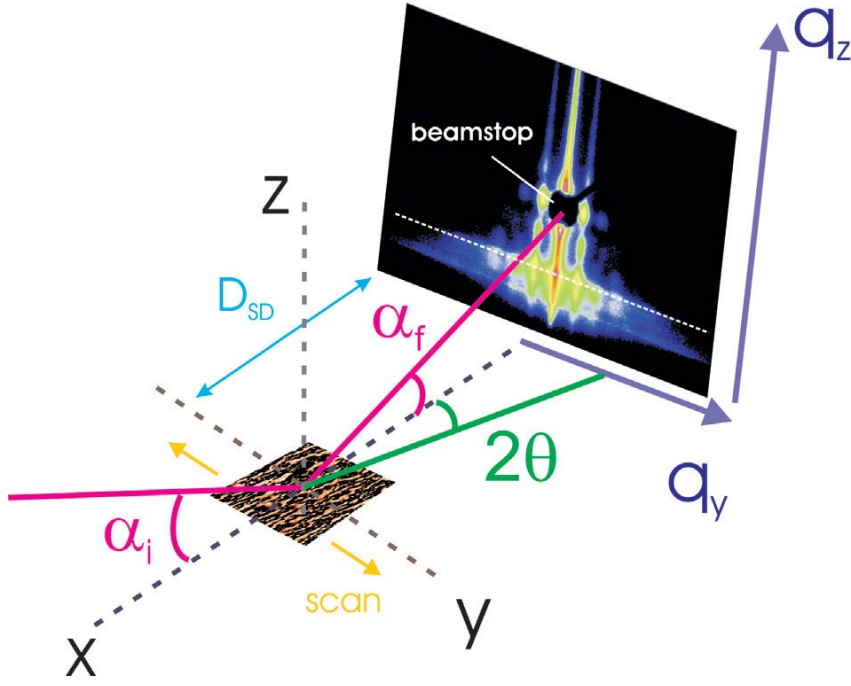


Fig. 1b. Sketch of the GISAXS geometry: a beamstop is used to protect the detector from the reflected beam which is much more intense than the diffuse scattering intensity. The white dashed line indicates the location of the out-of-plane cut.

We assume a fixed wavelength λ . Thus the monochromatic X-ray beam of wave vector k_i , with a wave number $k_0 = (2\pi)/(\lambda)$, is impinging onto the sample surface under an incident angle α_i and scattered under an exit angle α_f and an out of plane angle ψ . All these angles are typically smaller than 1 (in a range of a few tenth of degrees). Because of energy conservation, the X-ray beam is scattered along k_f and the scattering wave vector q defined by

$$q = (q_x, q_y, q_z) \quad (1)$$

with the components

$$q_x = 2\pi/\lambda [\cos(\psi)\cos(\alpha_f) - \cos(\alpha_i)], \quad (2)$$

$$q_y = 2\pi/\lambda [\sin(\psi)\cos(\alpha_f)], \quad (3)$$

$$q_z = 2\pi/\lambda [\sin(\alpha_i) + \sin(\alpha_f)] \quad (4)$$

For specular scattering, the wave vector components are $q_x = q_y = 0$ and $q_z \neq 0$, sampling a depth sensitive information only. With off-specular scattering, the lateral component is $q_{\parallel} = (q_x, q_y) \neq 0$ probing the in-plane structure of the sample.

In the experiment, the direct beam and the specular reflected beam are often suppressed by a beam stop to avoid the detector saturation as several orders of magnitude in intensity separate the diffuse scattering from the specular reflectivity [1]. As shown in Fig. 1b, it is advantageous to measure the GISAXS signal with a two dimensional (2d) detector. Typically the samples investigated with GISAXS were isotropic (2d powders), i.e., had

structures with a well-aligned axis perpendicular to the substrate and rotational averaging with respect to the surface normal, resulting in a rotationally homogeneous scattering intensity. The GISAXS pattern recorded on the 2d detector is symmetric with respect to the scattering plane. However, structures can show a preferential orientation with respect to the substrate, i.e., limiting cases such as gratings. In these cases, the GISAXS intensity distribution depends also on the azimuth angle ω of the substrate and the GISAXS pattern measured with the 2d detector is asymmetric with respect to the scattering plane.

Simulations

What is FitGISAXS?

FitGISAXS is a software package for performing modeling and analysis of GISAXS data within the distorted wave Born approximation (DWBA). The tool suite uses a slab-model approach with the Abeles matrix method to calculate X-ray reflectivity curves, electric field intensity distributions as well as GISAXS intensities from supported or buried scatterers arranged in 2 or 3 dimensions in a stratified medium. Models are included to calculate the scattered intensity for monodisperse, polydisperse, and interacting particles with various size distributions, form factors and structure factors. The source code for the entire package is freely available, allowing anyone to develop additional tools. [4]

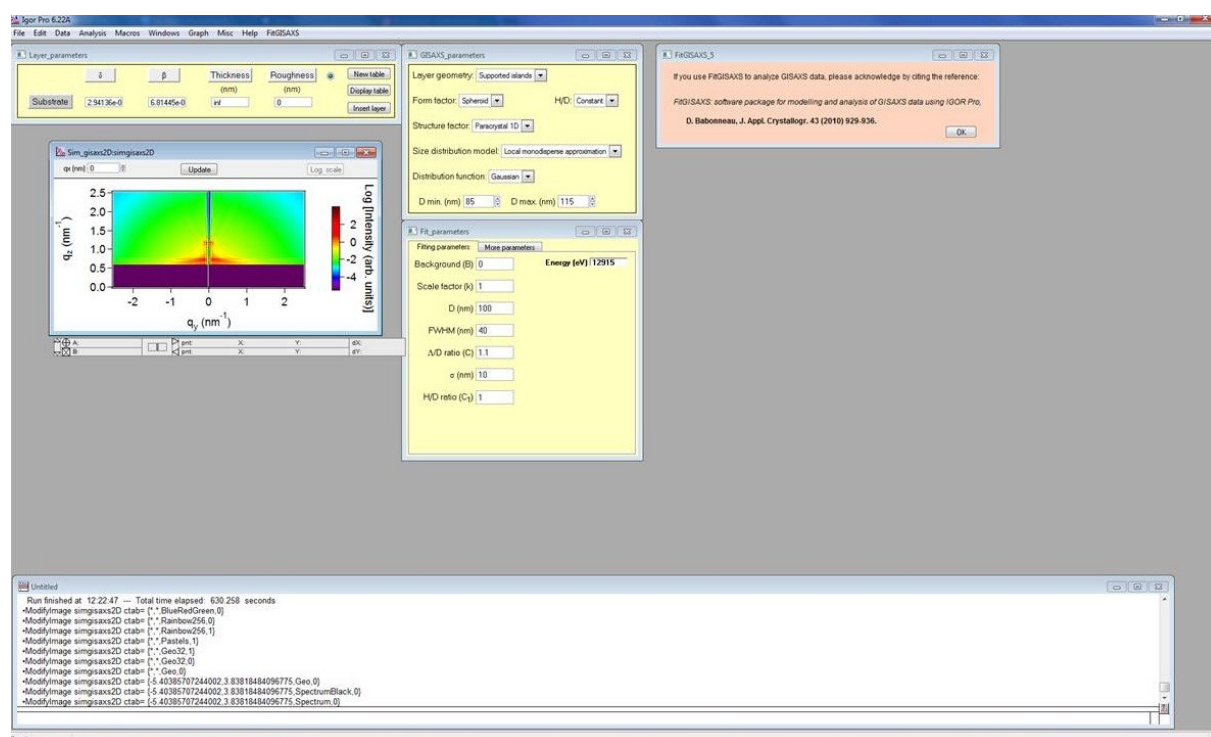


Fig. 2. A screen shot of the user interface.

As a result, 2D (Fig.3.) or 1D (Fig.4.) images are received. Comparing them with the experimental data can help understanding the process.

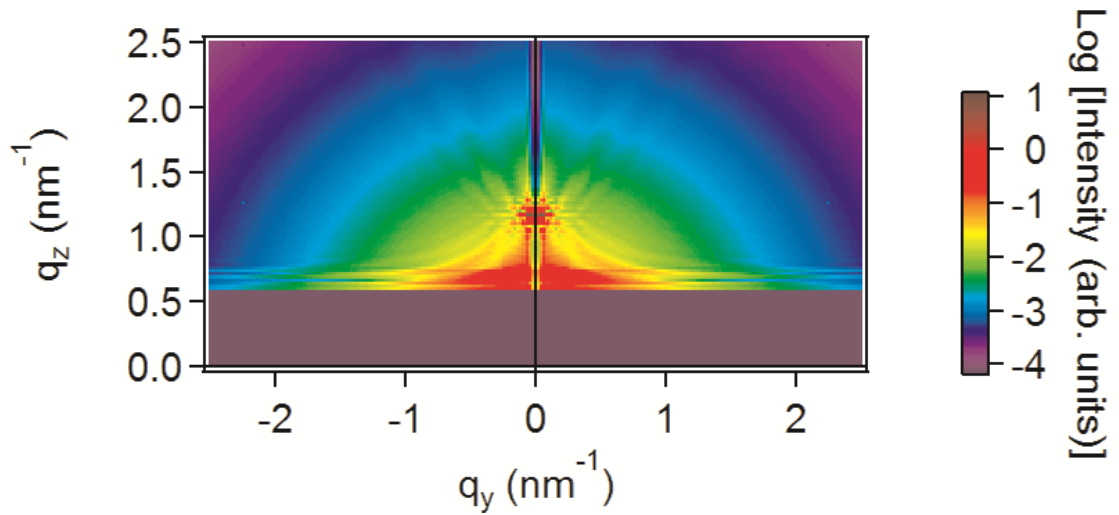


Fig. 3. 2D simulated GISAXS data

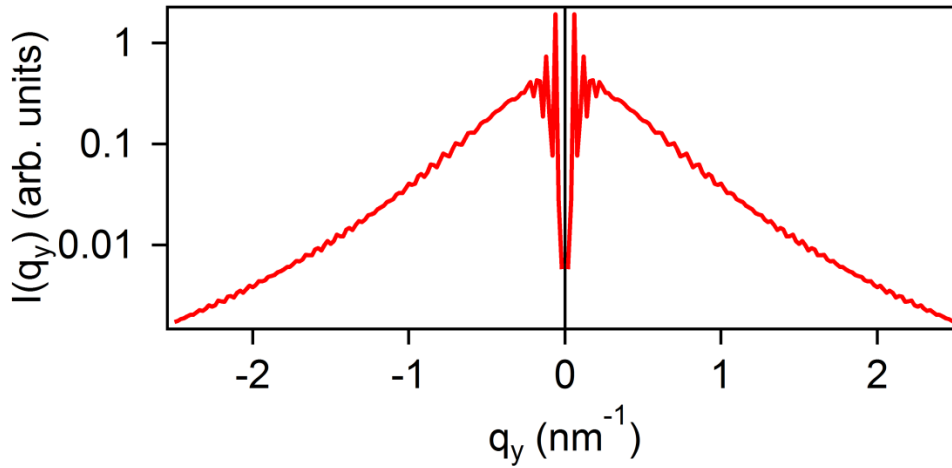


Fig. 4. 1D cut of GISAXS data as displayed

Experimental Data

Using GISAXS 2 samples were measured. Both of them have the structure of thin film with the substrate of silicon (Si). Using GLAD technique the layer of poly (styrene-block-isoprene) (PS) was produced in each of them. The only difference is that the sample 1 has only PS in its composition and the sample 2 has nanoparticles of gold (Au). In fig.5a the experimental data of the first sample is shown, in fig. 5b the Q_y -cut can be seen.

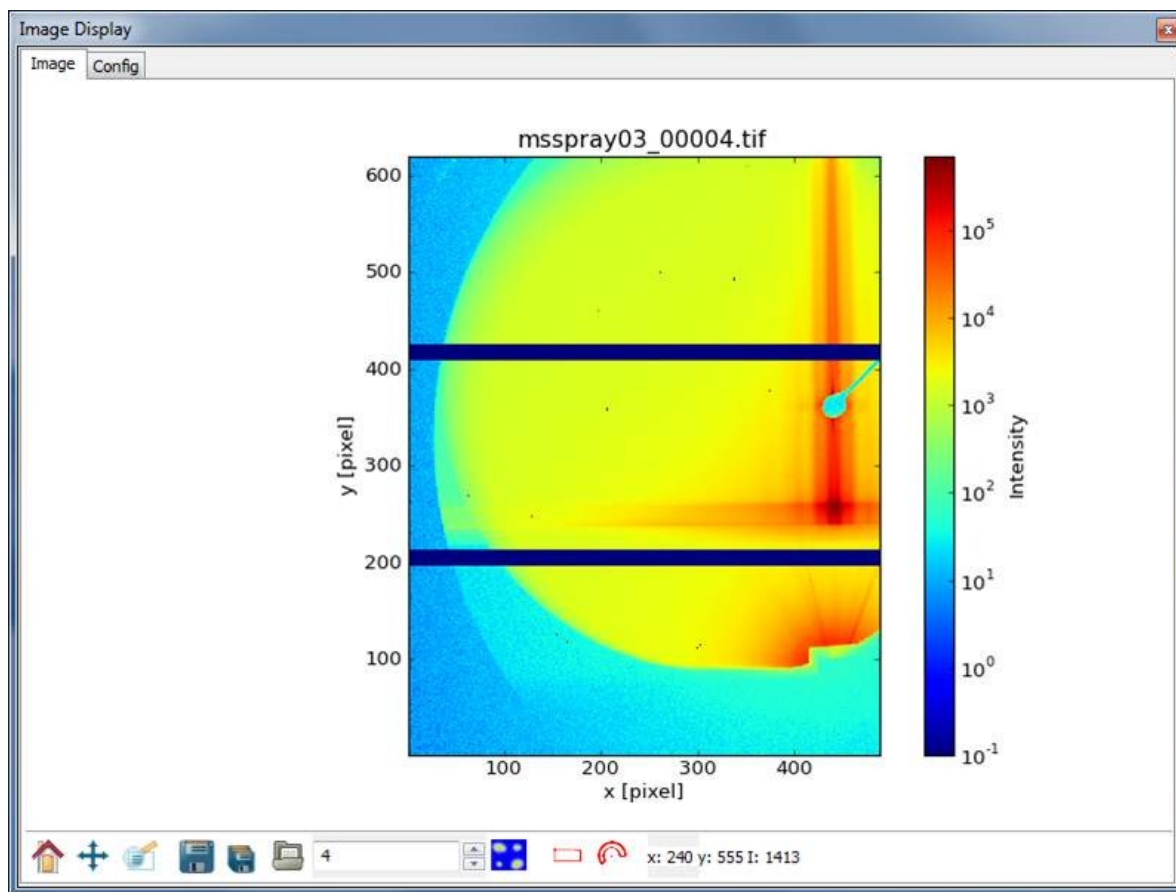


Fig.5a. 2D experimental data. Sample 1.

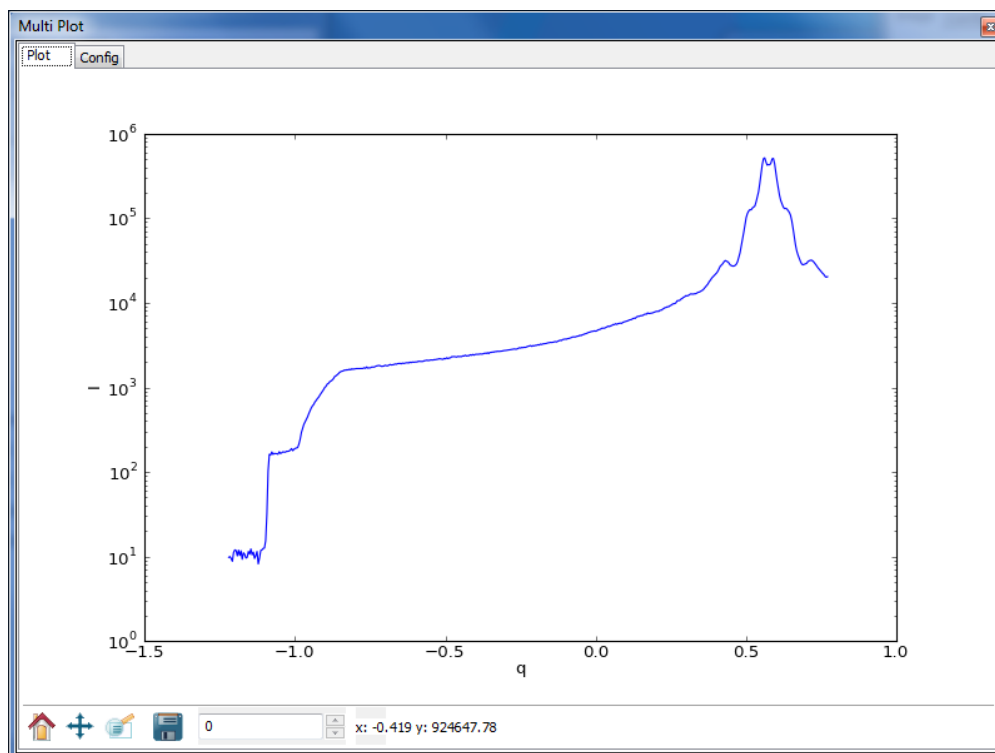


Fig.5b. 1D experimental data. Sample 1.

In fig.6a the experimental data of the second sample is shown, in fig. 6b the Qy-cut can be seen.

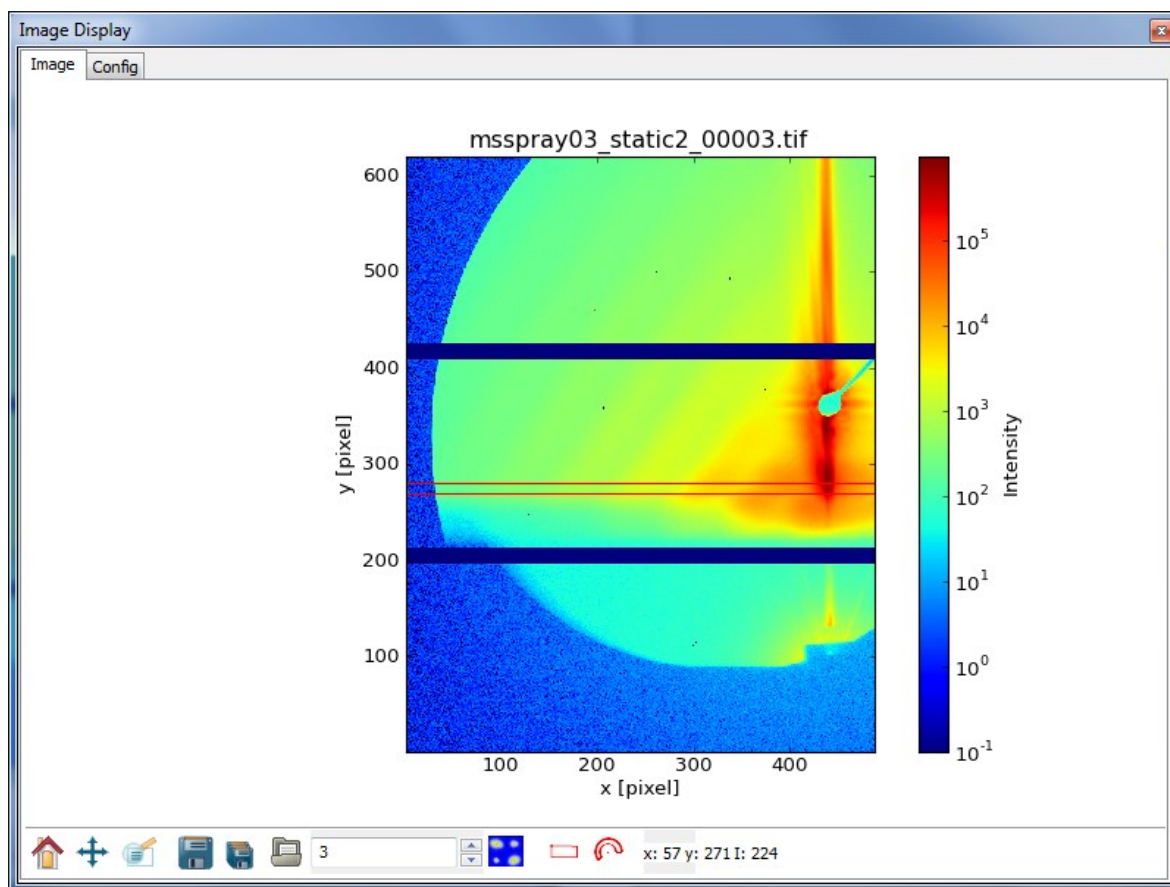


Fig.6a. 2D experimental data. Sample 2.

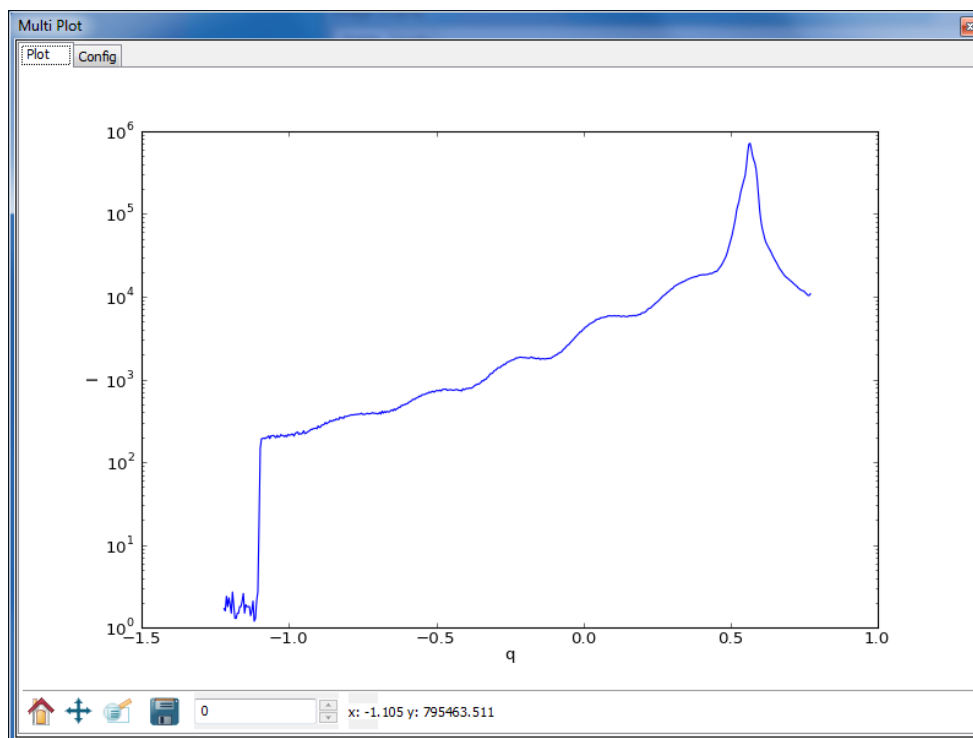


Fig.6b. 1D experimental data. Sample 2.

So the experimental data shows us the model which we should describe with the simulations.

Layer geometry: what to choose?

One of the main parameters which can be chosen is layer geometry. It shows the simplifications we use to describe the data. The following geometries are included in the FitGISAXS package:

- Born approximation
- Correlated roughness
- Supported Islands

Born approximation consists of taking the incident field in place of the total field as the driving field at each point in the scatterer. The Born approximation is simplest when the incident waves are plane waves. That is, the scatterer is treated as a perturbation to free space or to a homogeneous medium. Accordingly, refraction, reflection, and absorption effects are not taken into account in the calculation. [5] The scattering amplitude in the Born approximation is given by

$$f(\theta, \varphi) = -\frac{\mu}{2\pi\hbar^2} \int e^{-i\vec{k}\cdot\vec{r}'} V(\vec{r}') \phi_{inc}(\vec{r}') d^3r' = -\frac{\mu}{2\pi\hbar^2} \int e^{i\vec{q}\cdot\vec{r}'} V(\vec{r}') d^3r',$$

The Born approximation is valid for large incident energies and weak scattering potentials. In other words, the Born approximation is valid at low energies provided the potential is well below the strength necessary for a bound state.

In Fig.7 it is showed that Born approximation (on the left) is not very similar to the experimental data (on the right). So another geometry should be used.

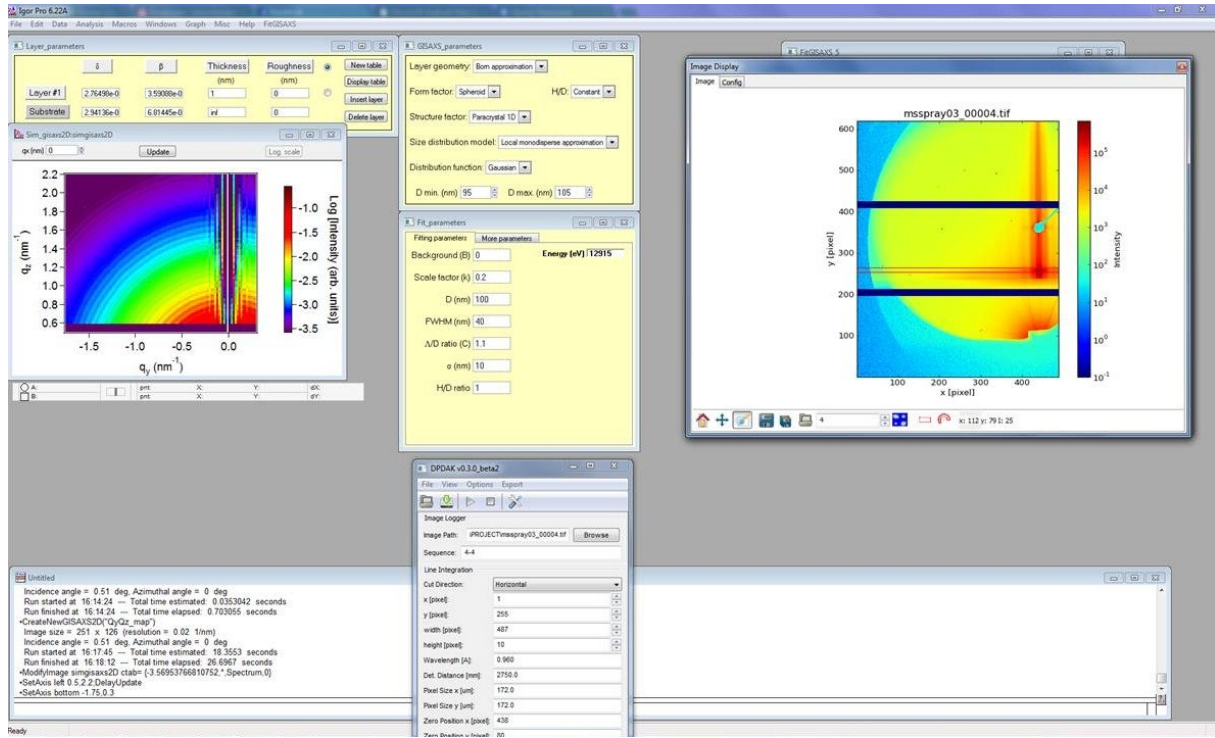


Fig.7. 2D simulated data using layer geometry “Born approximation” (on the left) and comparison to the experimental data (on the right).

Correlated roughness is another one to be applied. In it the form factor is calculated by assuming that it originates from a 2D assembly of scatterers located at the interface z_{j+1} of a stratified medium and that their lateral positions are perfectly replicated to the surface roughness ($z_1 = 0$). Accordingly, the total scattered intensity is the sum of three terms describing (i) the intensity scattered by the objects located at the interface z_{j+1} ,

(ii) the intensity scattered by the objects located at the interface z_1 ,

(iii) the interference between them 6 :

$$|F(q)|^2 = |F_j(q)|^2 + |F_0(q)|^2 + 2|F_j(q)||F_0(q)|\cos(q_z z_{j+1})$$

where $F_j(q)$ is the form factor of the buried scatterers and $F_0(q)$ is the form factor of the surface scatterers. [4]

In Fig.8 the layer geometry as “Correlated roughness” is shown. As it can be noticed, the experimental data is so different to the simulated that another one should be found.

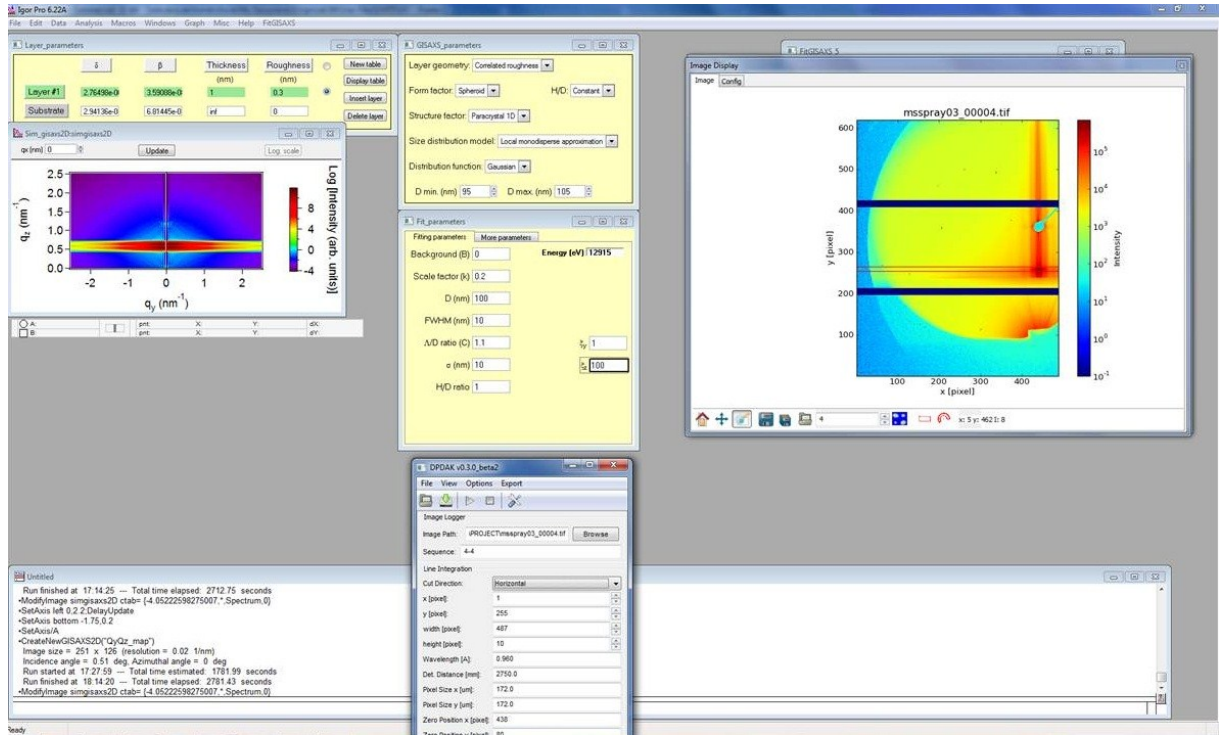


Fig.8. 2D simulated data using layer geometry “Correlated roughness” (on the left) and comparison to the experimental data (on the right).

Supported islands is the layer geometry in which the form factor is calculated applying to a 2D assembly of scatterers located at the interface z_{j+1} of a stratified medium. Form factor can be described by the following:

$$F(q_{\parallel}, k_z^i, k_z^f) = F(q_{\parallel}, k_z^f - k_z^i) + R_F(\alpha_i) F(q_{\parallel}, k_z^f + k_z^i) + R_F(\alpha_f)$$

$$F(q_{\parallel}, -k_z^f - k_z^i) + R_F(\alpha_i) R_F(\alpha_f) F(q_{\parallel}, -k_z^f + k_z^i).$$

In Fig.9 the layer geometry as “Supported islands” is shown. It is easily to find that this simulated data describes the experimental data very well. So this is the best layer geometry that can be found in this software.

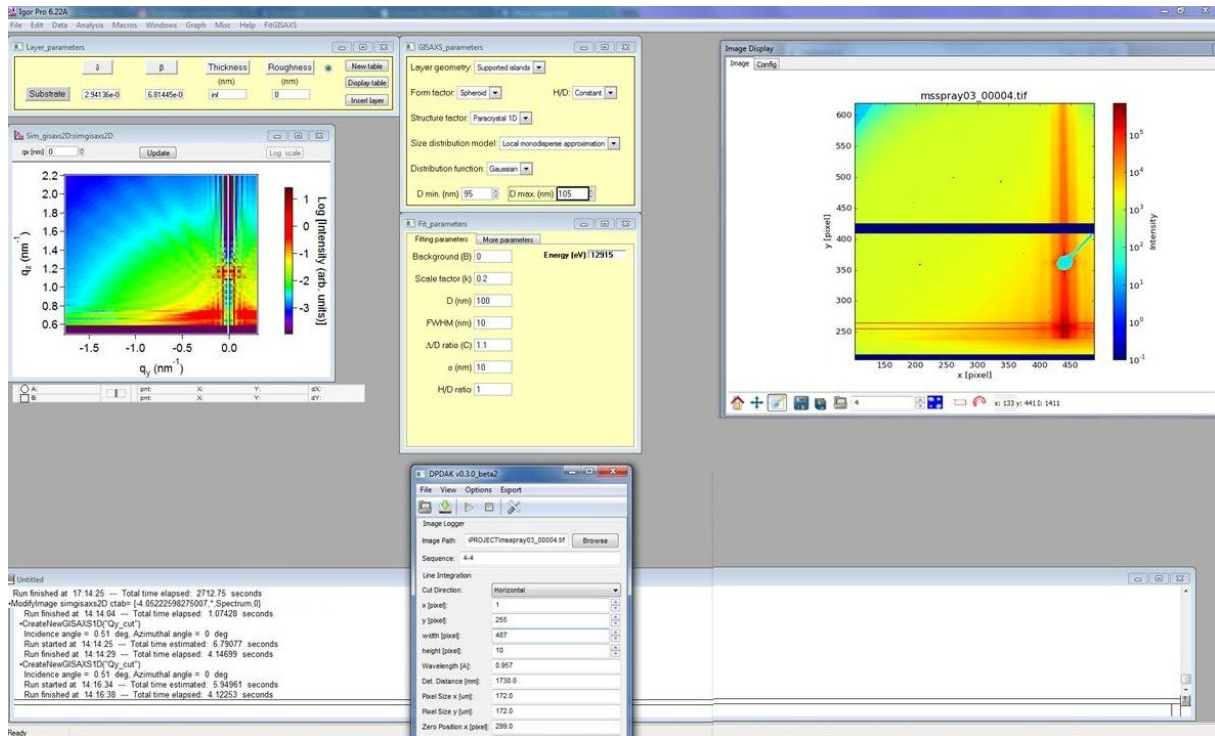


Fig.9. 2D simulated data using layer geometry “Supported islands” (on the left) and comparison to the experimental data (on the right).

Size distribution models

What else should be chosen for better fitting the experimental data is size distribution model. There are some most-used types:

- Monodisperse approximation (MA)
- Decoupling approximation (DA)
- Local monodisperse approximation (LMA)

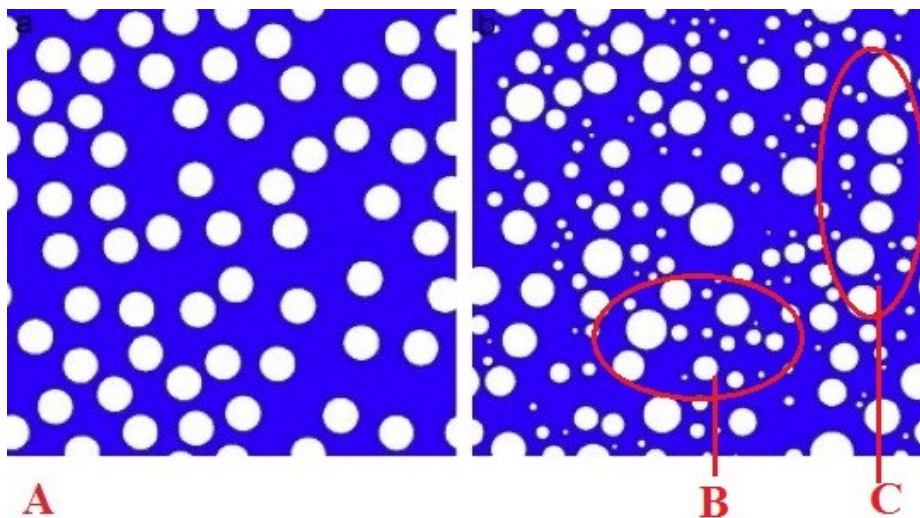


Fig.10. Size distribution models: A – Monodisperse Approximation (MA), B – Decoupling Approximation (DA), C – Local Monodisperse Approximation (LMA).

Monodisperse approximation (MA) (Fig. 10A) is the ideal model that describes the situation when all the particles are the same size and shape and the distance between particles is very similar within the reference accuracy. It is such an ideal model that we can't use to describe our experimental data.

A current hypothesis called **Decoupling Approximation** (DA) (Fig.10B) is to suppose that the kind of the scatterers and their positions are not correlated in such a way that the partial pair correlation functions depend only on the relative positions of the scatterers (homogeneous system). For instance, this hypothesis is justified for isotopic disorder in the field of neutron scattering. For particles, this approximation is restricted to dilute systems. A factorization becomes possible

$$\left(\frac{d\sigma}{d\Omega}\right)_{part} = \Phi_0(q_{\parallel}) + | \langle \mathcal{F}(q_{\parallel}, k_{inz}, k_{scz}) \rangle |^2 S(q_{\parallel})$$

$$S(q_{\parallel}) = 1 + n_s \int_A (g(r_{\parallel}) - 1) e^{iq_{\parallel}r_{\parallel}} dr_{\parallel}$$

$S(q_{\parallel})$ – the so-called total interference function is the Fourier transform of the particle position autocorrelation function irrespective of the kind of the particle.[7]

In Fig.11 the simulated data is displayed. It is easy to see that the experimental data looks similar to the simulated, but all peaks in both vertical and horizontal directions are not all the same.

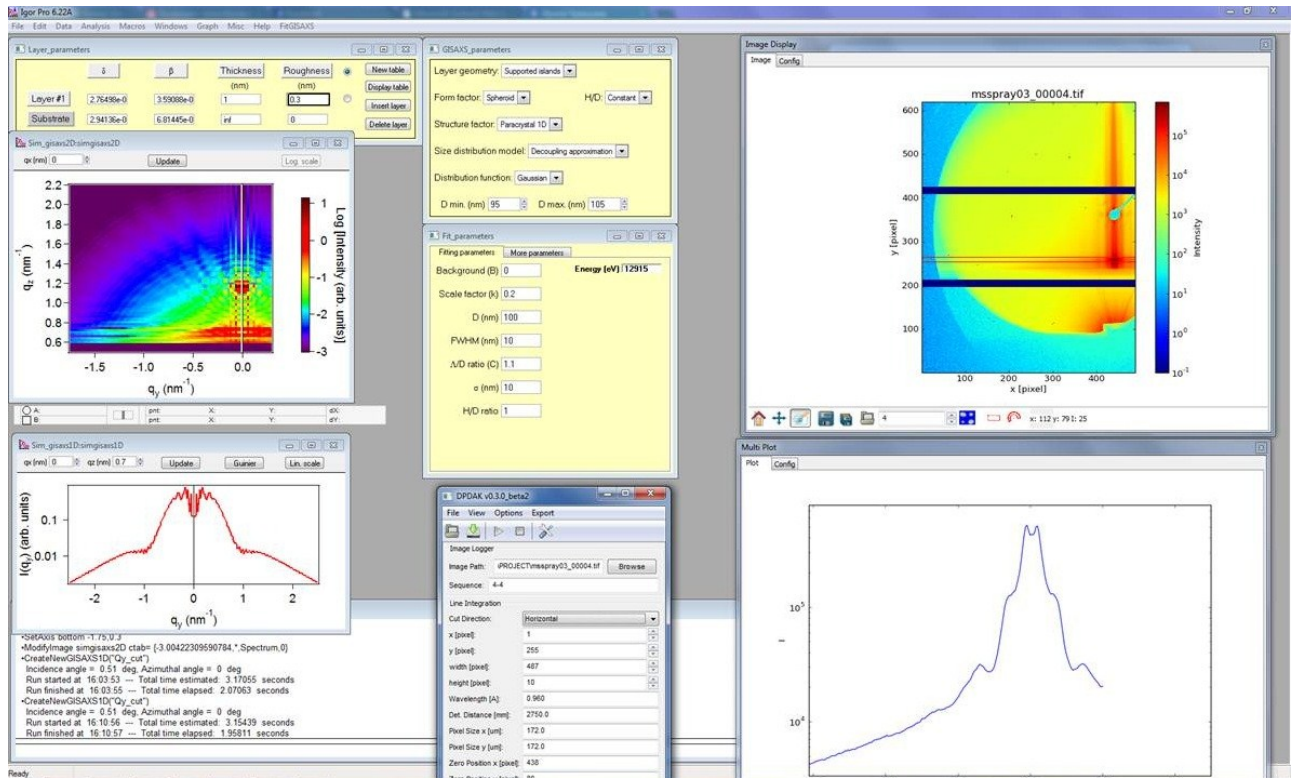


Fig.11. 2D simulated data using Decoupling approximation (on the left) and comparison to the experimental data (on the right).

In Fig.12 the cuts of both experimental and simulated data are presented. The difference between them can be noticed easily, especially the second peaks of the simulated data are wrong. So to sum up, this approximation is good but we should find better one.

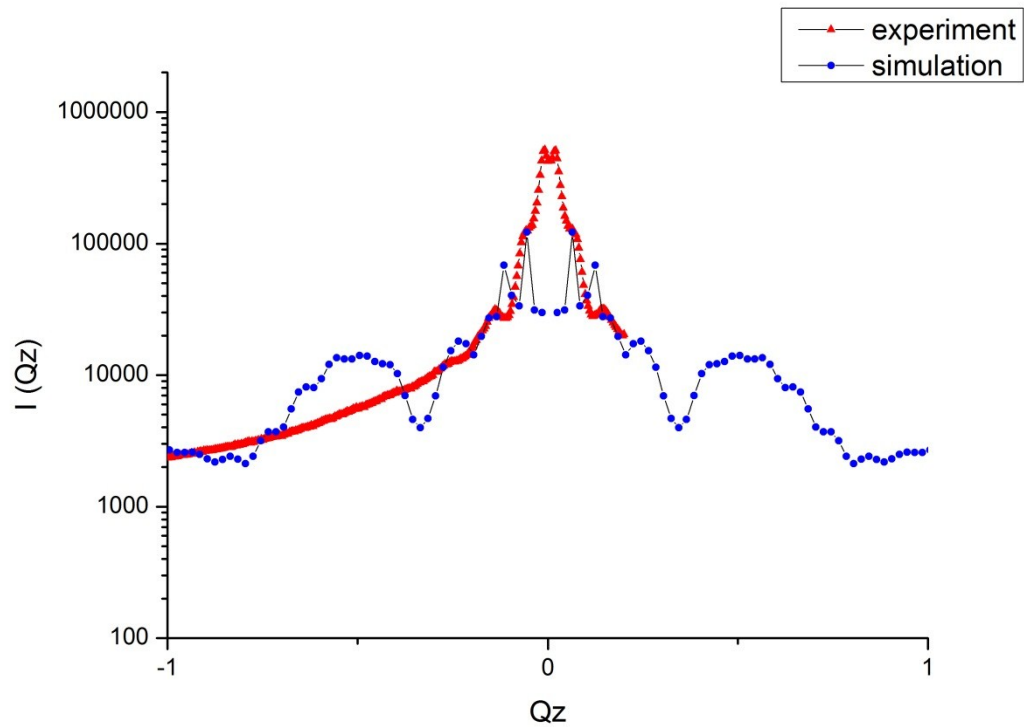


Fig.12. 1D simulated data using Decoupling approximation (blue line) and comparison to the experimental data (red line).

Local monodisperse approximation (LMA) (Fig.10C) is the hypothesis widely used in the literature which assumes that the system is made of locally monodisperse domains that interfere incoherently. The particle-particle pair correlation function can vary from domain to domain. In other words, the surrounding of each particle is supposed to be made of particles of the same size and shape in such a way that the particle kind varies slowly across the sample but with a spatial wavelength lower than the coherence of the beam. The cross section reads

$$\left(\frac{d\sigma}{d\Omega}\right)_{part} = \langle |\mathcal{F}_\alpha(q_{\parallel}, k_{inz}, k_{scz})|^2 S_\alpha(q_{\parallel}) \rangle$$

It works nicely on a point of view of data analysis because partial correlation between particles can be reintroduced in each domain. But, one has to bear in mind that LMA relies on an unphysical description of most of the experimental systems. Upon a progressive increase of the size correlation between neighboring particles, a continuous transition from DA to LMA is obtained.[7]

In Fig.13 the simulated data is displayed. It is easy to see that the experimental data looks very similar to the simulated, and almost all peaks in both vertical and horizontal directions are the same. Even in Fig.14 where the cuts of both experimental and simulated data are presented it can be noticed. The difference between them can be recognized easily. However, the difference is much lighter than in the decoupling approximation. So this approximation describes the experimental data in the best way.

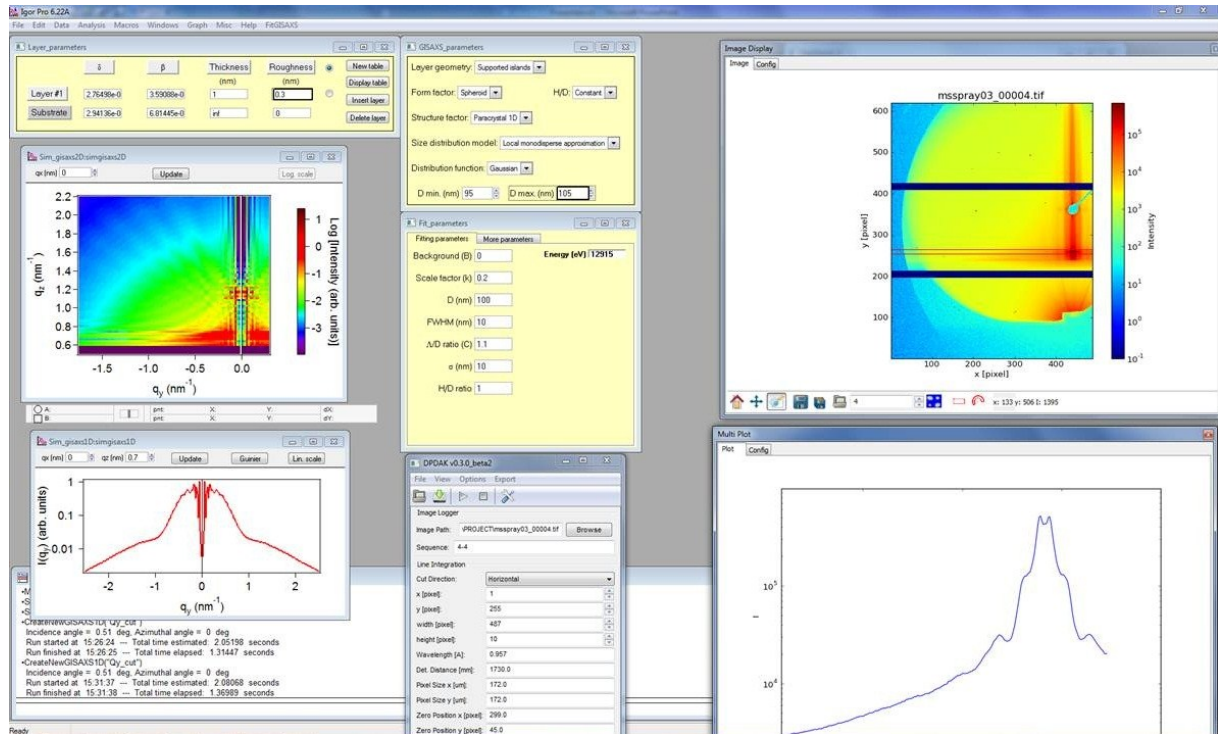


Fig.13. 2D simulated data using Local Monodisperse approximation (on the left) and comparison to the experimental data (on the right).

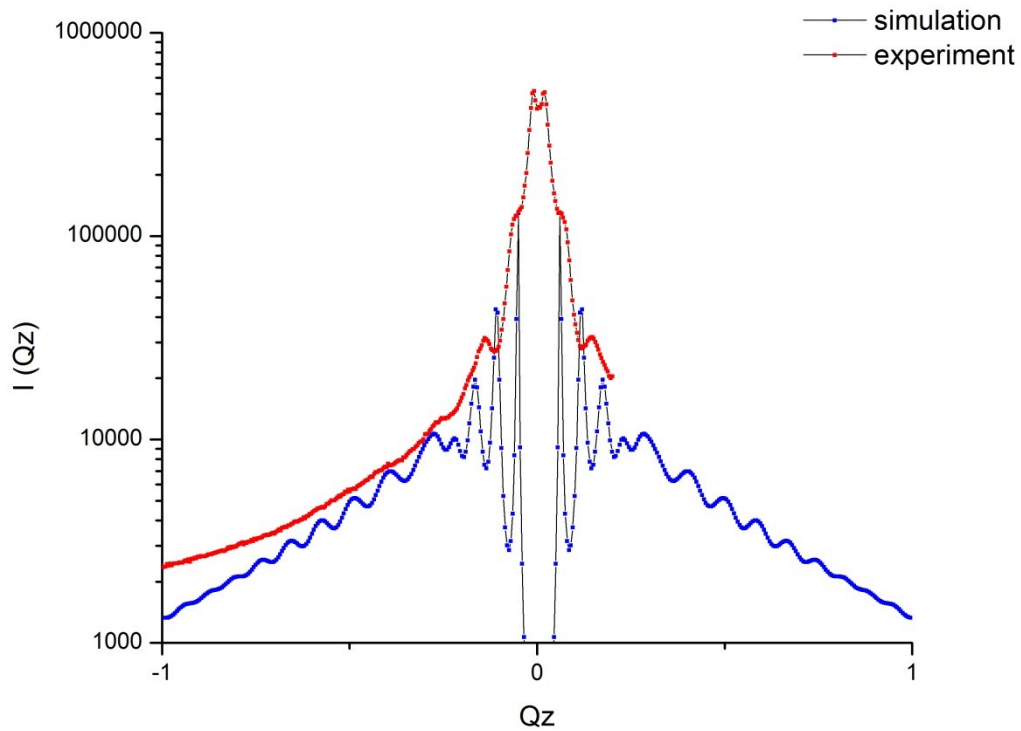


Fig.14. 1D simulated data using Local Monodisperse approximation (blue line) and comparison to the experimental data (red line).

To sum up, two main parameters for describing the experimental data have been chosen. As a layer geometry, it is better to use “Supported Islands” and as a size distribution model – LMA.

Other parameters

Despite the layer geometry and size distribution model, other parameters should be chosen to describe the experimental data in the best way.

Structure factor

Structure factor is also very important parameter. The best that can suit our experimental data are:

- Random organization
- Paracrystal 1D

The first one, **Random organization**, shows the situation when the scatterers are considered as isolated objects.

As it is shown in fig. 15 and fig.16 this structure factor doesn't fit anything in the experimental data so it is out of use for this situation.

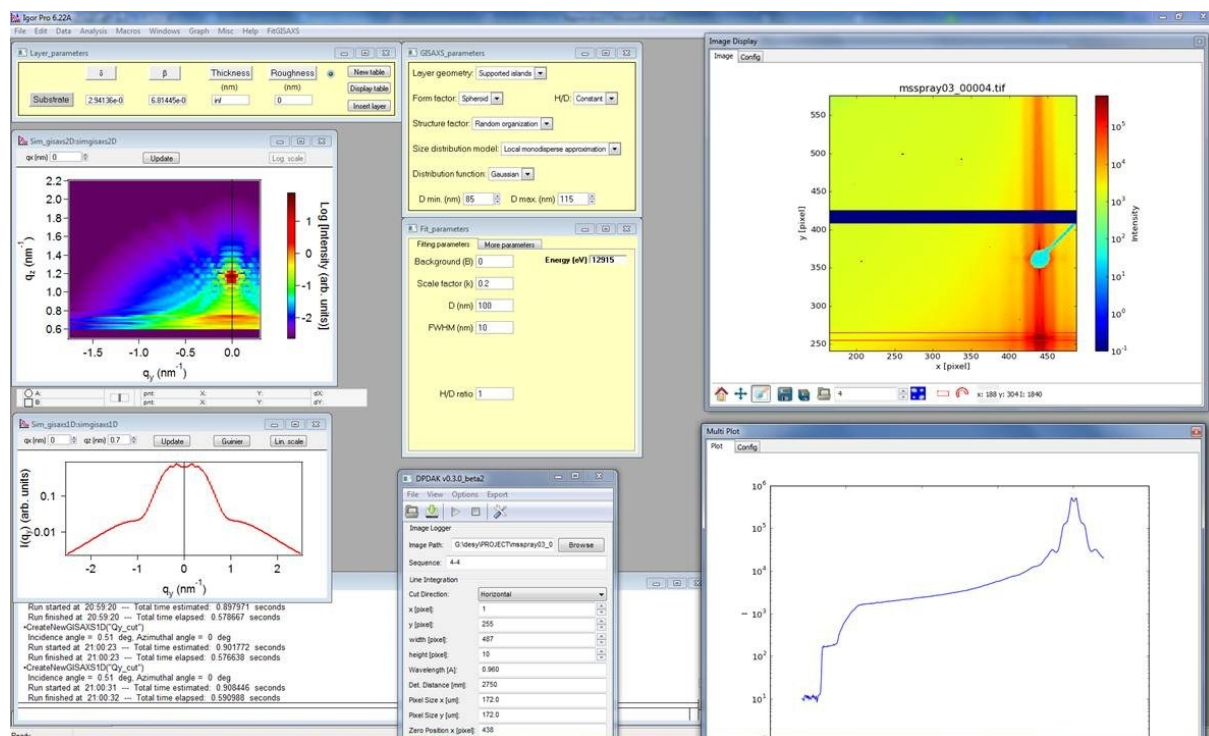


Fig.15. 2D simulated data using Random organization as a structure factor (on the left) and comparison to the experimental data (on the right).

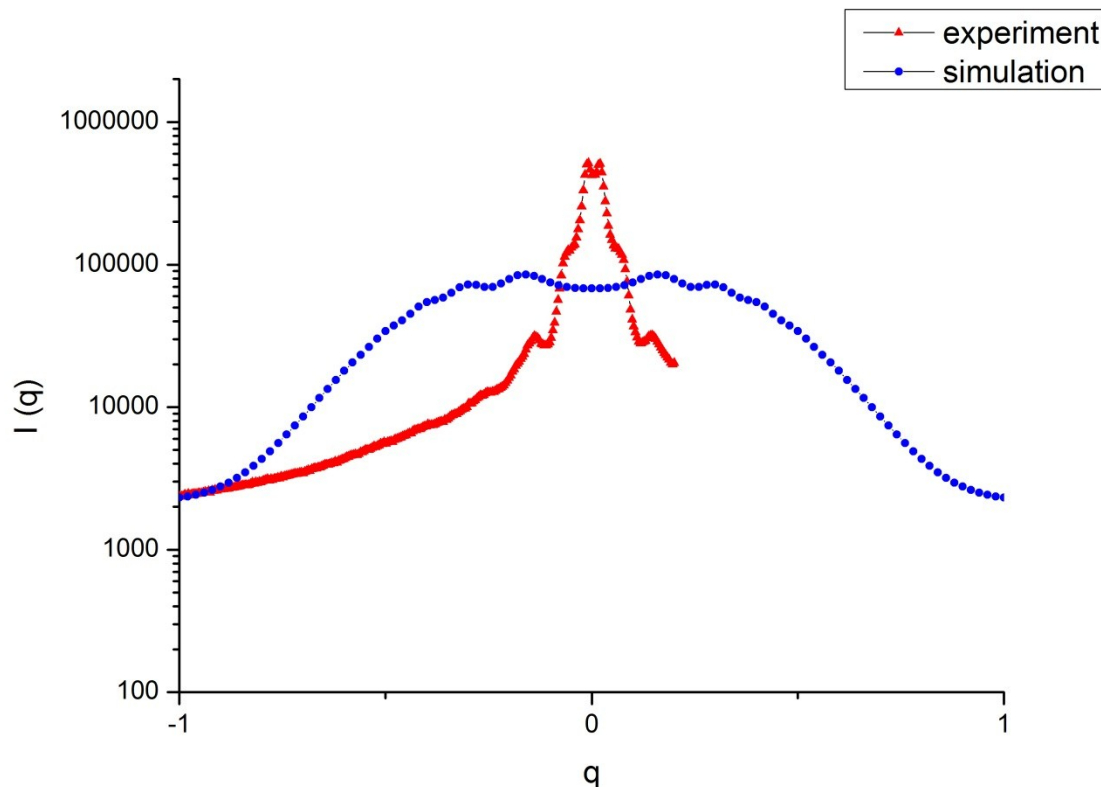


Fig.16. 1D simulated data using Random organization as a structure factor (blue line) and comparison to the experimental data (red line).

In the second one, **Paracrystal 1D**, the structure factor is calculated within the paracrystal theory. [6] The mean interparticle distance, Λ , is assumed to be proportional to D with a constant factor C ($\Lambda = C \times D$) and the standard deviation is σ .

$$S(q_y) = \frac{1 - \exp(-q_y^2 \sigma^2)}{1 - 2 \exp\left(-\frac{1}{2} q_y^2 \sigma^2\right) \cos(q_y \Lambda) + \exp(-q_y^2 \sigma^2)}$$

As it is shown in fig.17, the simulated data looks like the experimental and the cuts on the fig.18 confirm it.

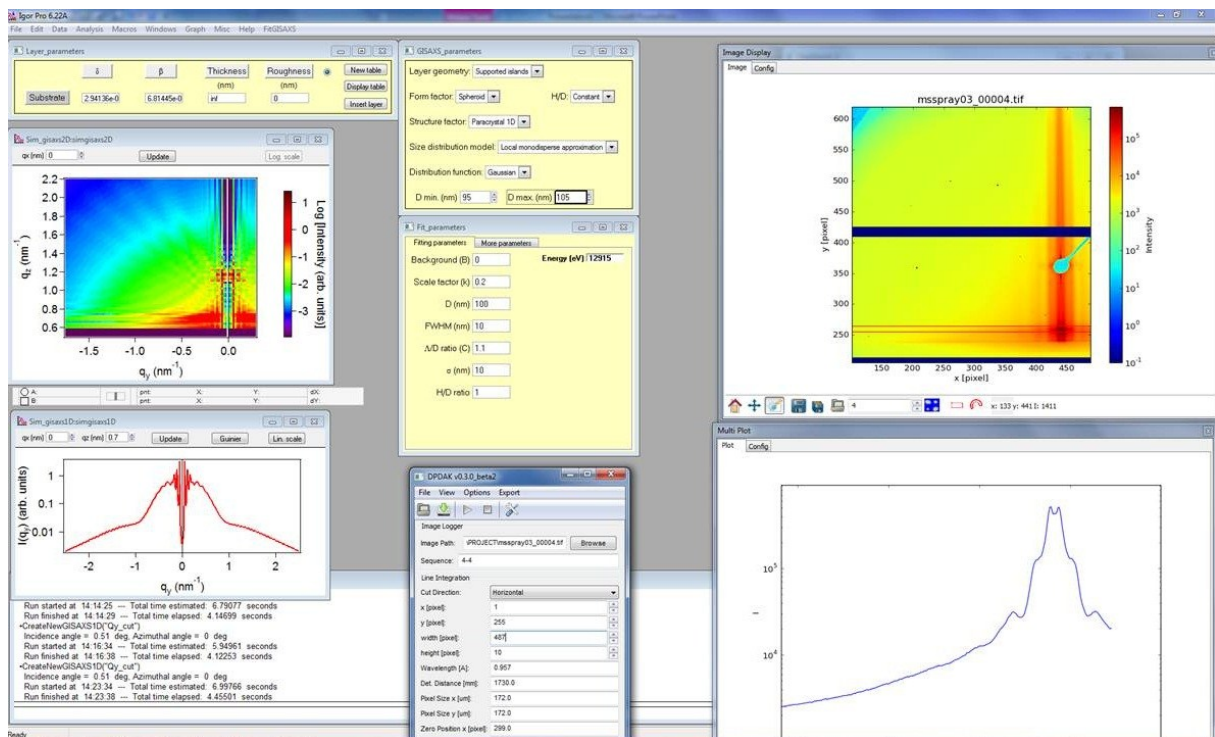


Fig.17. 2D simulated data using Paracrystal 1D as a structure factor (on the left) and comparison to the experimental data (on the right).

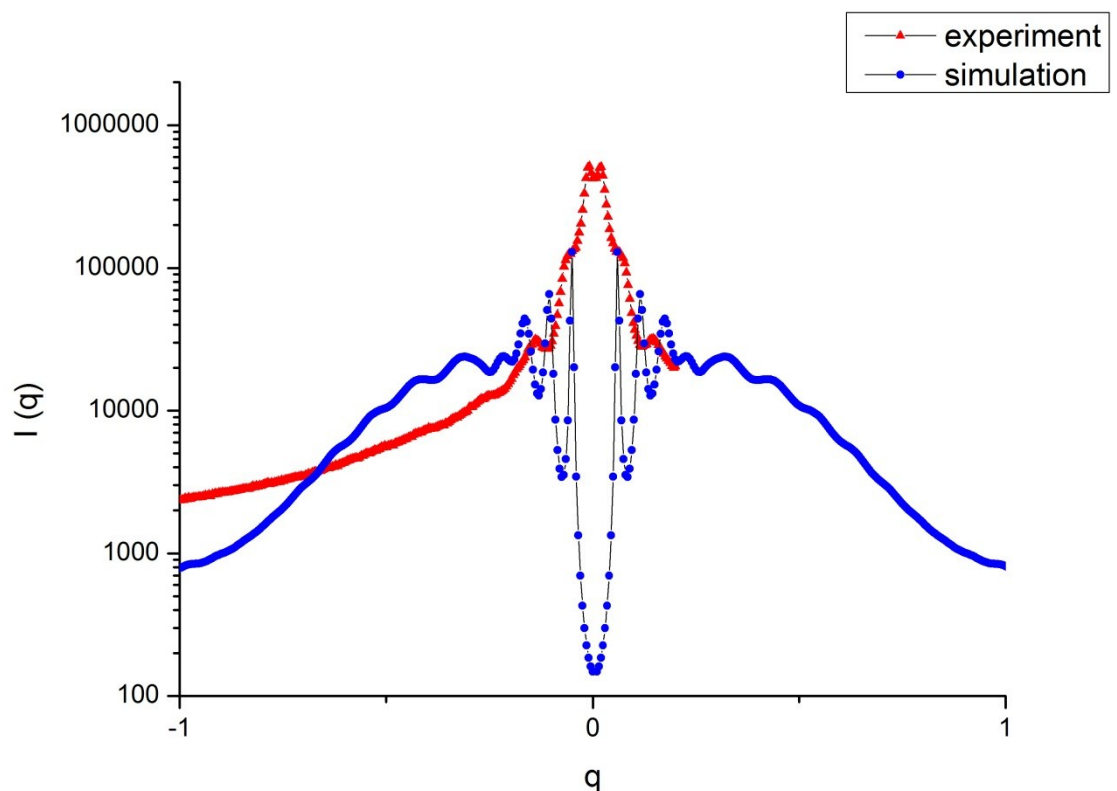


Fig.18. 1D simulated data using Paracrystal 1D as a structure factor (blue line) and comparison to the experimental data (red line).

So this approximation describes the experimental data in the best way.

Form factor

As in the experimental data two samples are presented, so two form factors should be chosen.

For the first stage, there are no other variants except for spheroid because as it can be seen in the SEM the particles have spheroid shape. And fig.17 and fig.18 confirm that it fits well.

For the last stage (second sample) there are some options:

- Tilted ellipsoids
- Tilted hemispheres
- Tilted cylinders

The **tilt angle** could be 35 or 55 degrees. At fig.19 and fig 20 the cylinders with the tilt angle of 35 degrees are presented.

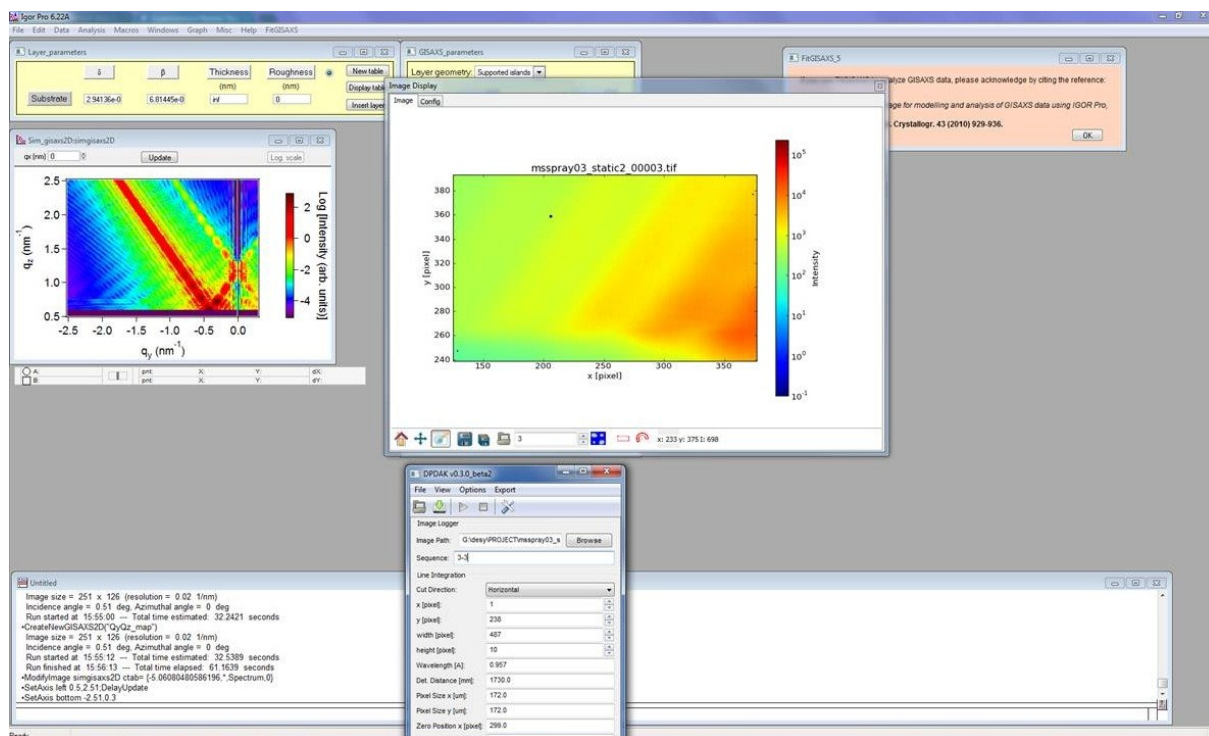


Fig.19. 2D simulated data using Cylinders with the tilt angle of 35 degrees as a form factor (on the left) and comparison to the experimental data (on the right).

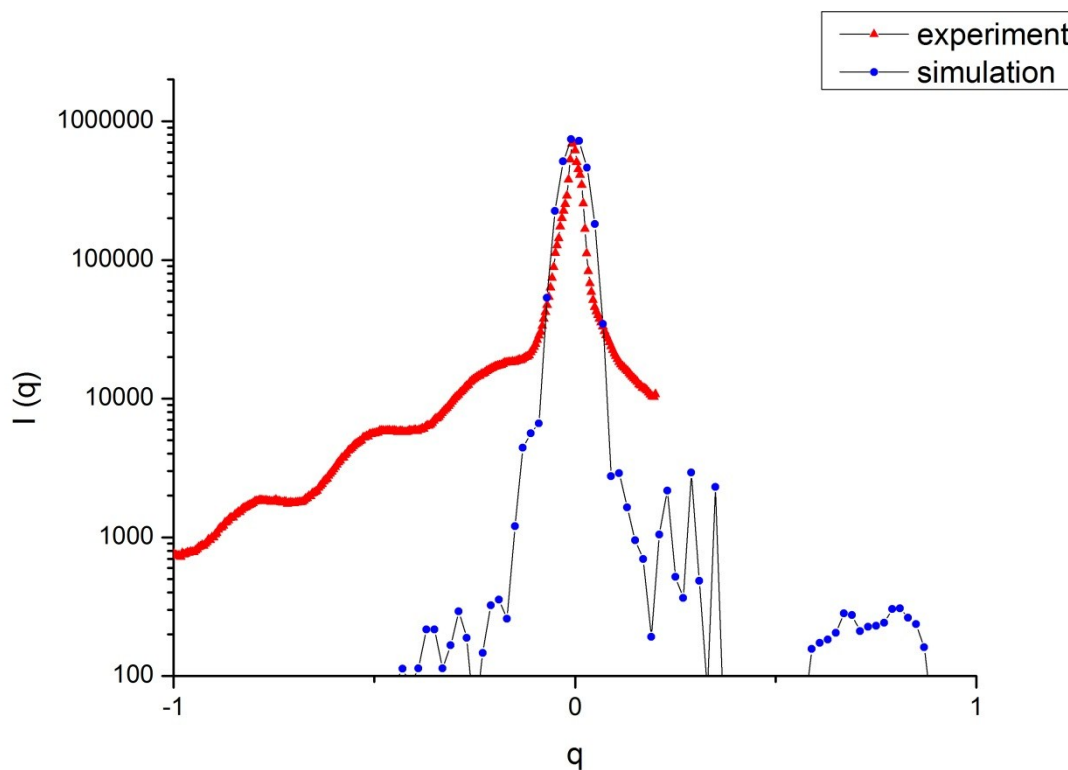


Fig.20. 1D simulated data using Cylinders with the tilt angle of 35 degrees as a form factor (blue line) and comparison to the experimental data (red line).

And at the fig.21 and fig. 22 the same cylinders with the tilt angle of 55 degrees are presented.

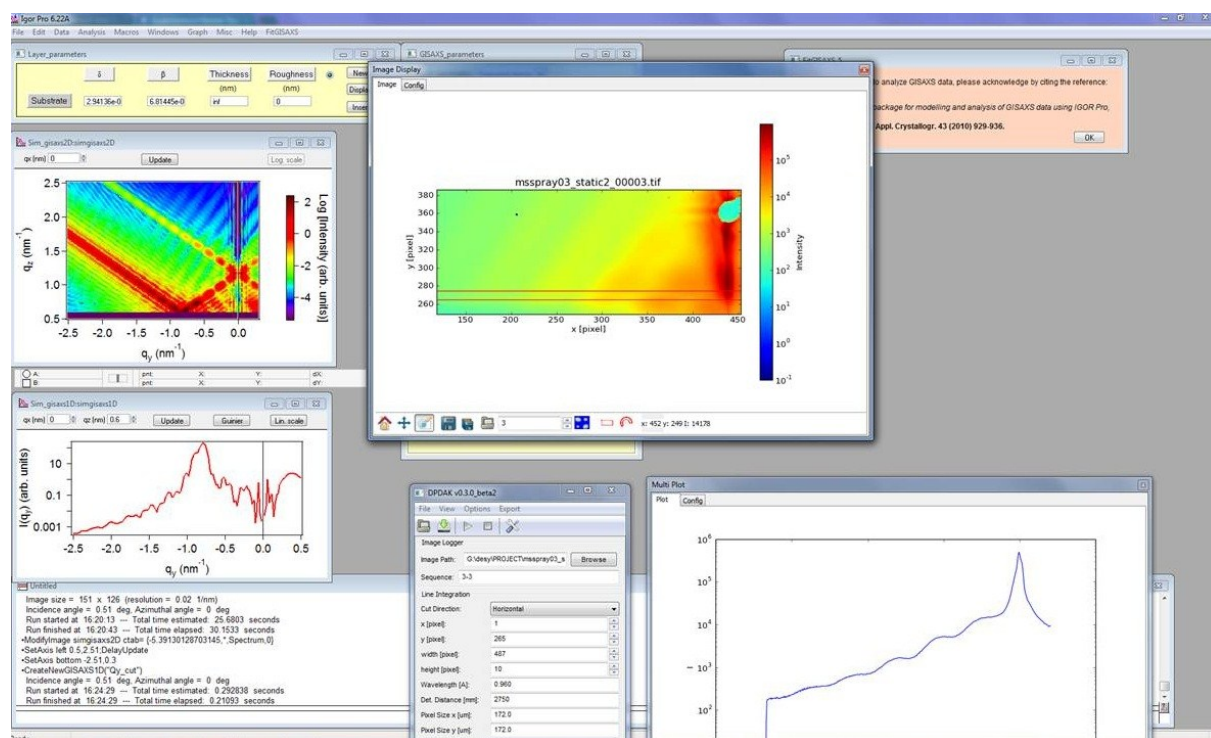


Fig.21. 2D simulated data using Cylinders with the tilt angle of 55 degrees as a form factor (on the left) and comparison to the experimental data (on the right).

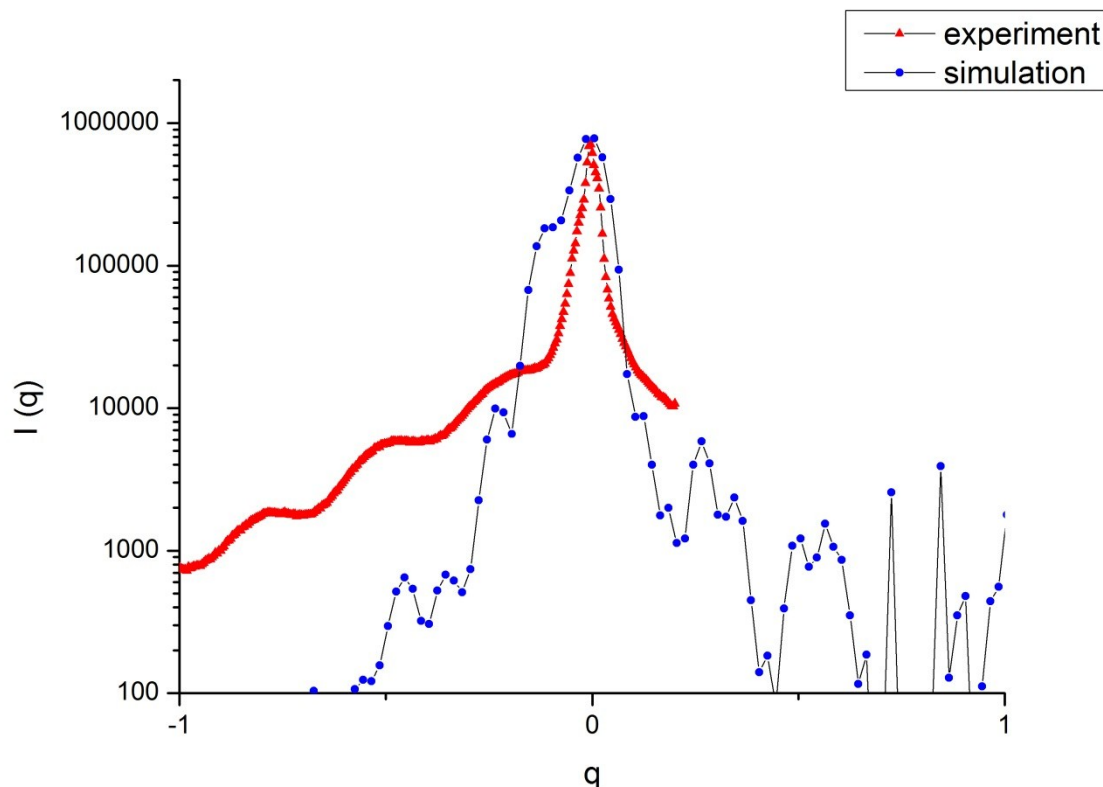


Fig.22. 1D simulated data using Cylinders with the tilt angle of 55 degrees as a form factor (blue line) and comparison to the experimental data (red line).

So it can be easily noticed that the right angle is 55 degrees.

After choosing the right angle, the right form factor should be chosen.

First of all, **tilted ellipsoids** should be examined.

At fig. 23 and fig. 24 they are presented.

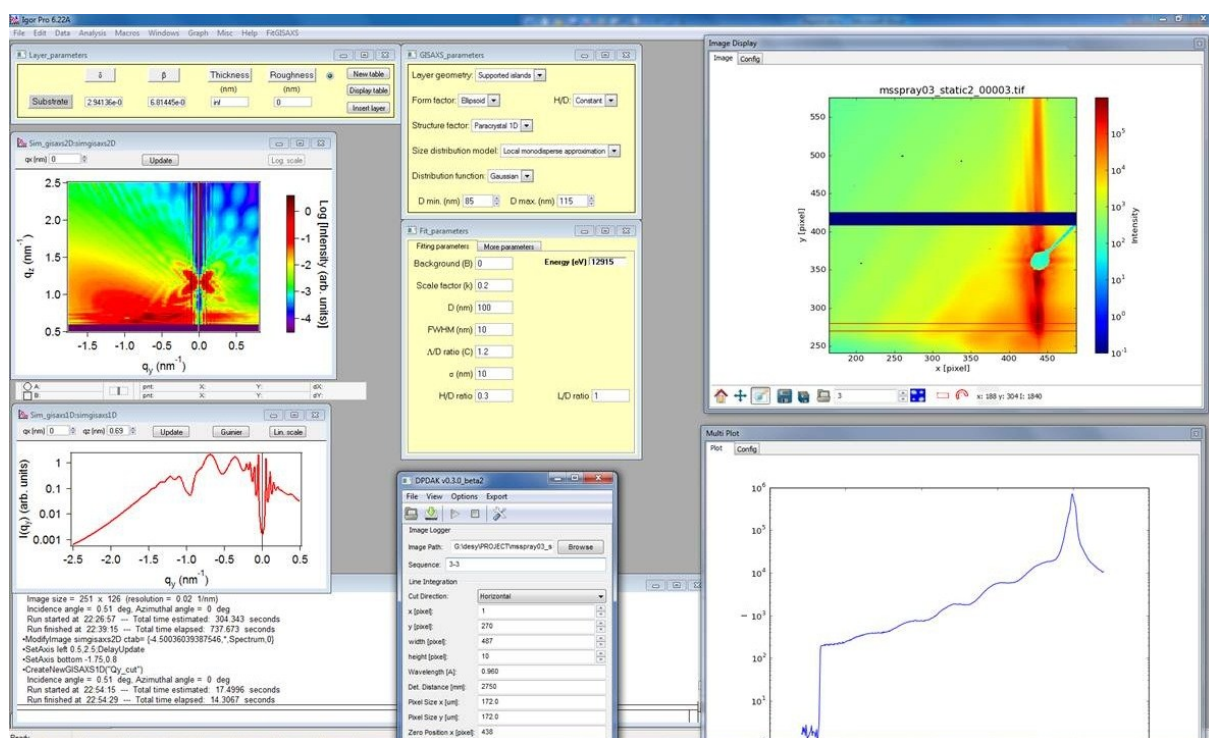


Fig.23. 2D simulated data using Tilted ellipsoids as a form factor (on the left) and comparison to the experimental data (on the right).

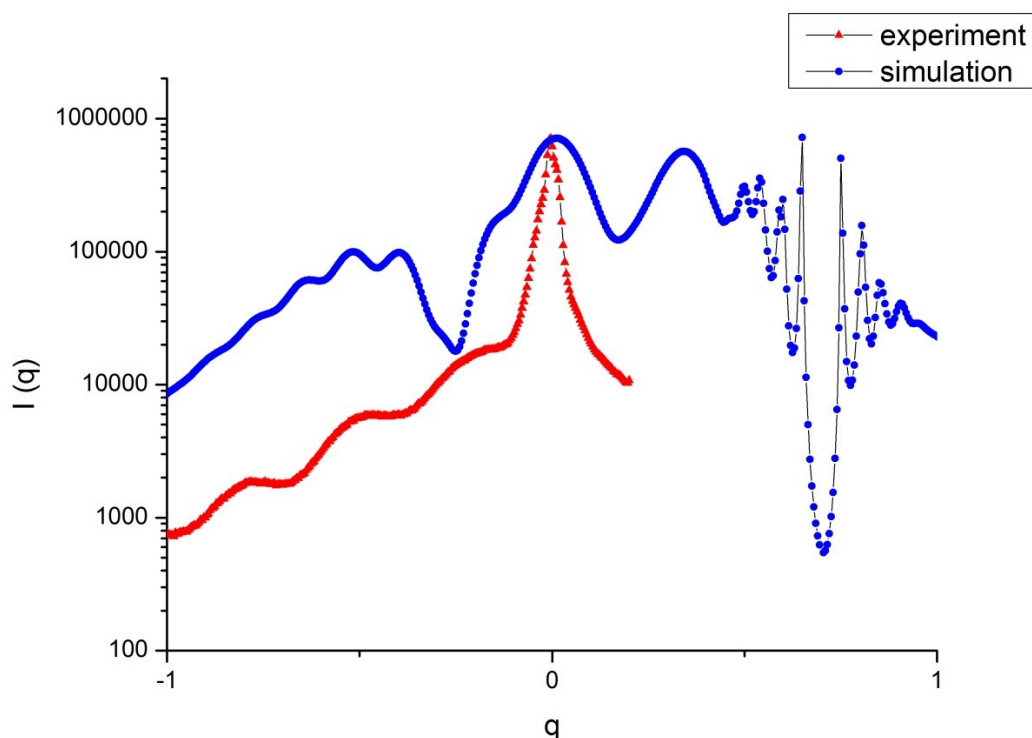


Fig.24. 1D simulated data using Tilted ellipsoids as a form factor (blue line) and comparison to the experimental data (red line).

It is seen that the experimental and simulated data are completely different. So this model doesn't suit our data well.

Then the **tilted hemispheres** should be looked at.

At fig. 25 and fig. 26 the hemispheres with Height/Diameter=0.15 are presented.

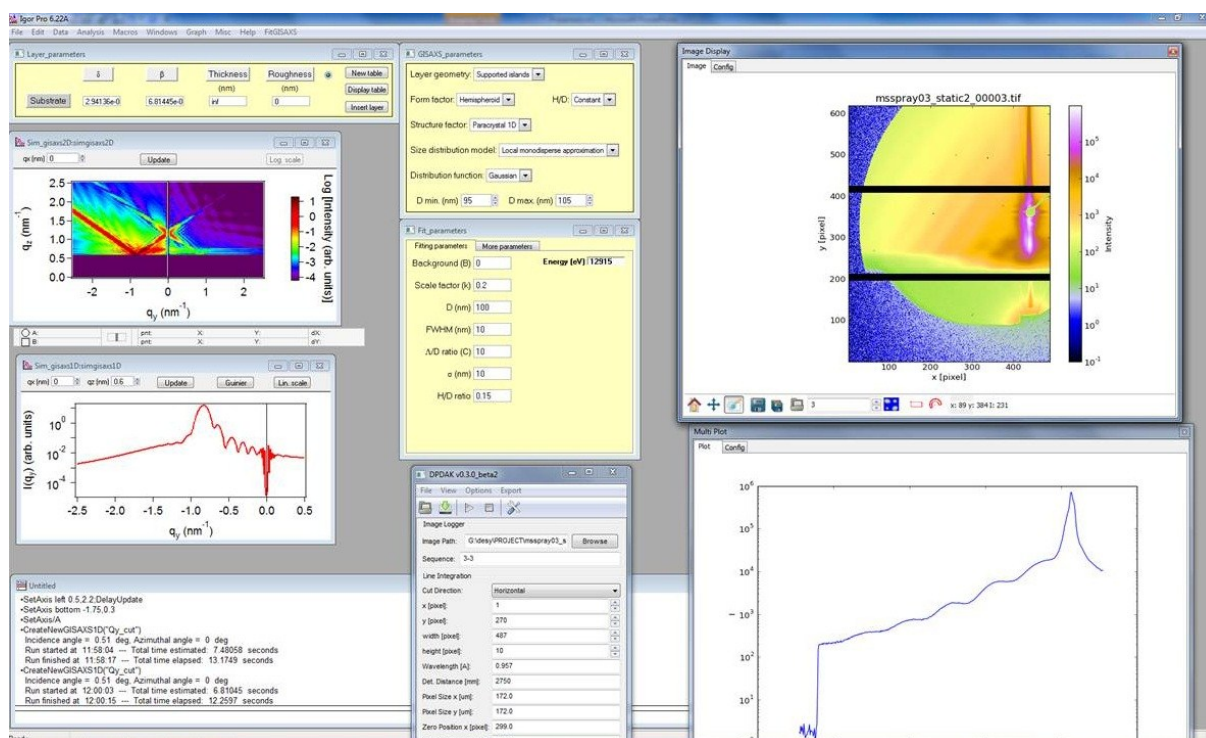


Fig.25. 2D simulated data using Tilted hemispheres ($H/D=0.15$) as a form factor (on the left) and comparison to the experimental data (on the right).

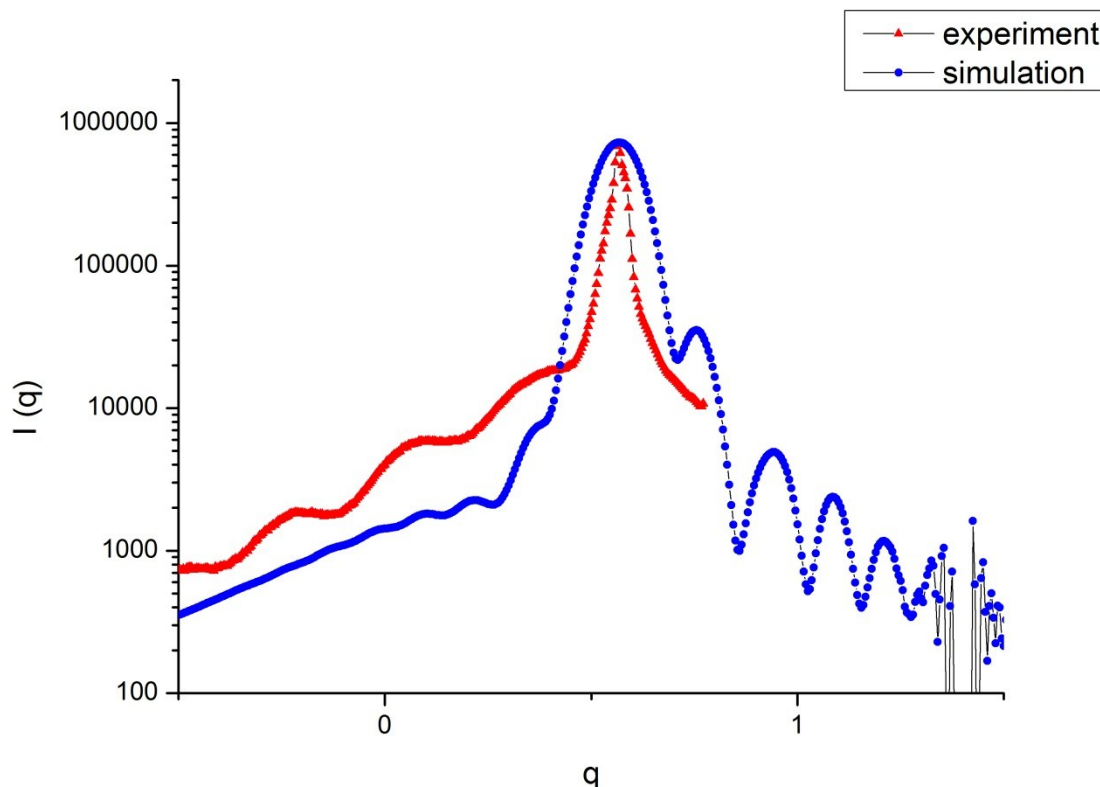


Fig.26. 1D simulated data using Tilted hemispheres ($H/D=0.15$) as a form factor (blue line) and comparison to the experimental data (red line).

At fig. 27 and fig. 28 the hemispheres with Height/Diameter=0.20 are presented.

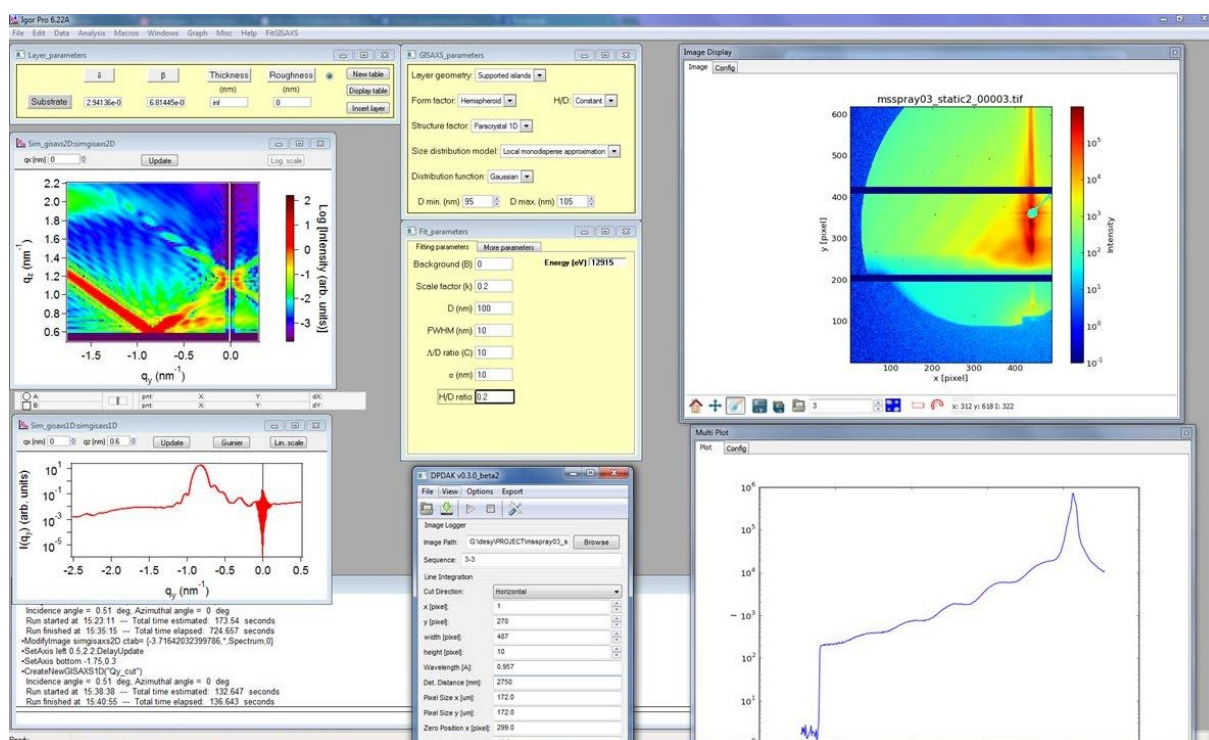


Fig.27. 2D simulated data using Tilted hemispheres (H/D=0.20) as a form factor (on the left) and comparison to the experimental data (on the right).

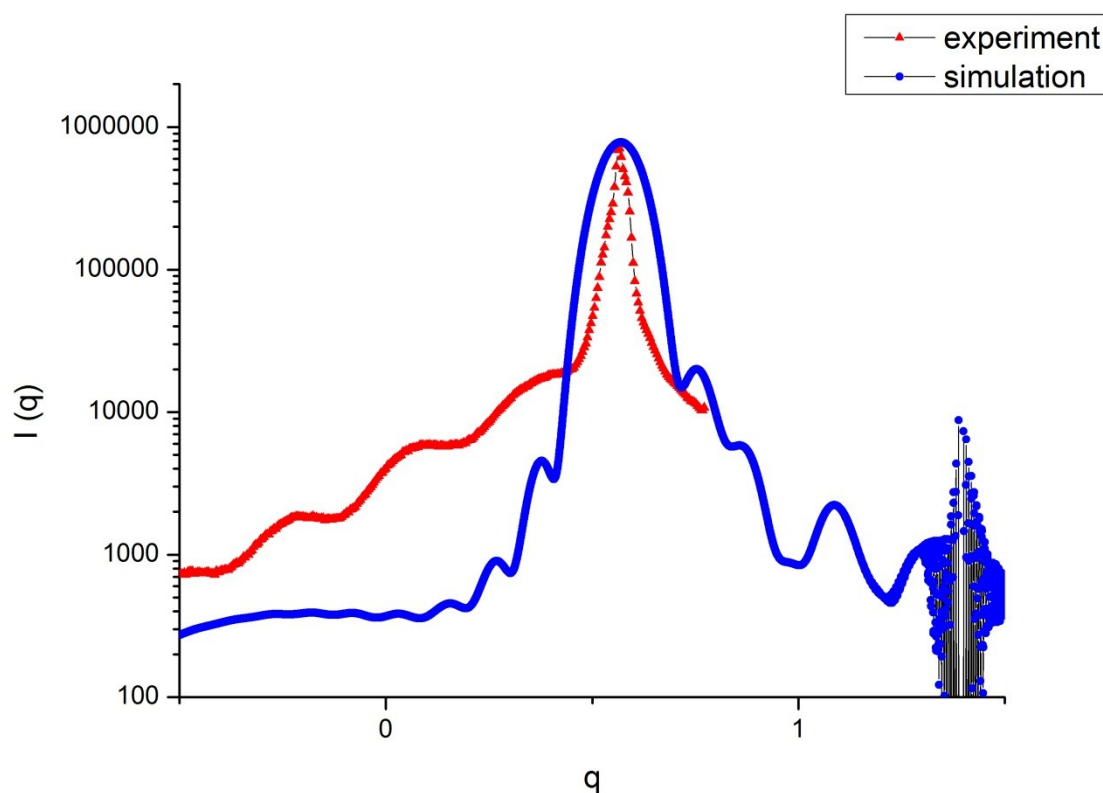


Fig.28. 1D simulated data using Tilted hemispheres (H/D=0.20) as a form factor (blue line) and comparison to the experimental data (red line).

At fig. 29 and fig. 30 the hemispheres with Height/Diameter=0.25 are presented

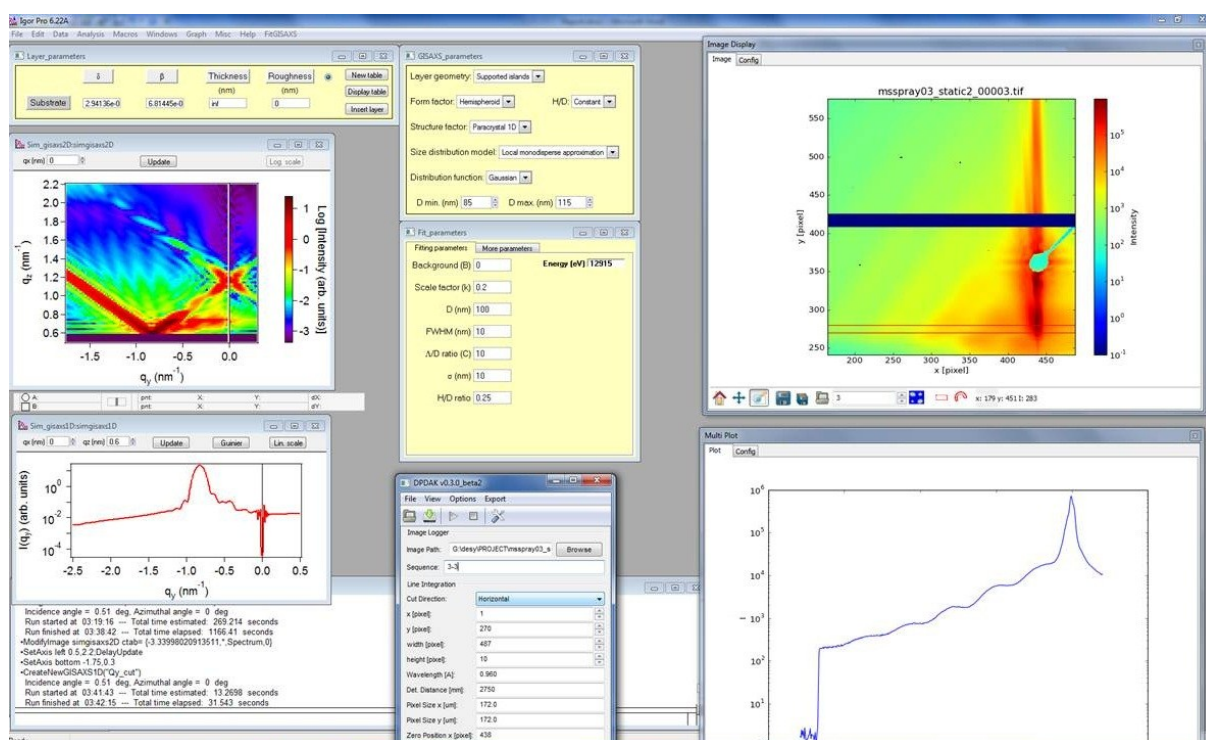


Fig.29. 2D simulated data using Tilted hemispheres ($H/D=0.25$) as a form factor (on the left) and comparison to the experimental data (on the right).

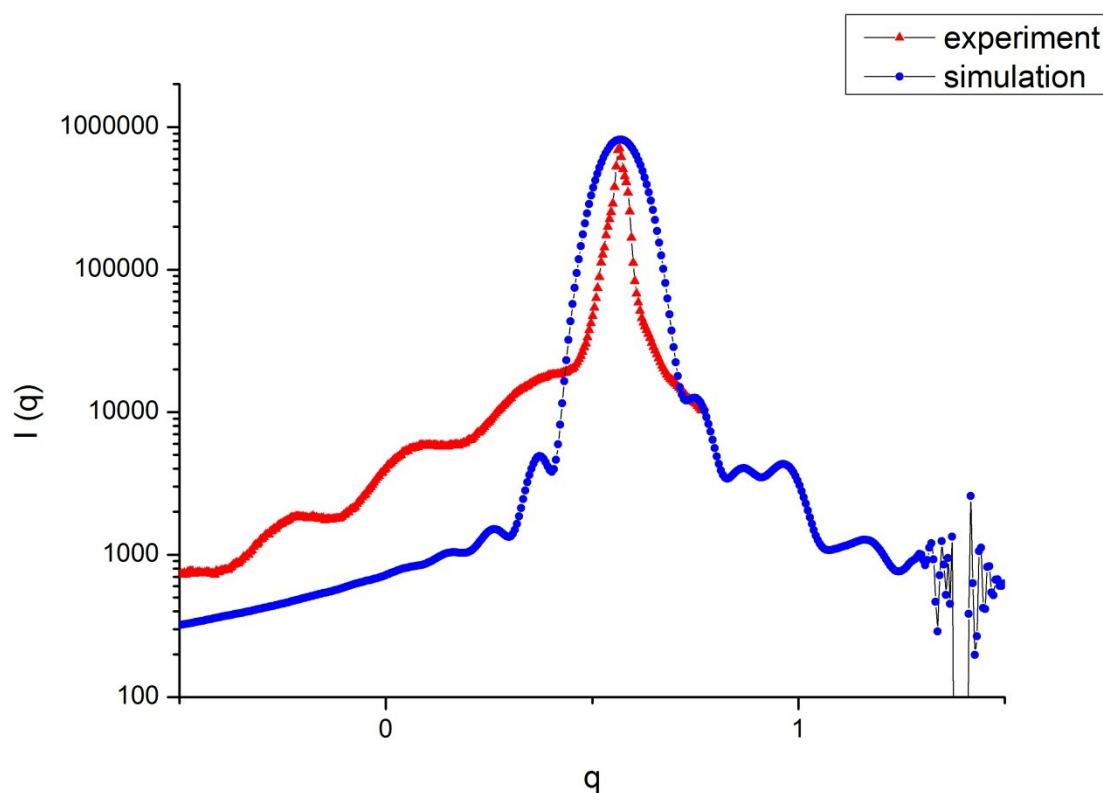


Fig.30. 1D simulated data using Tilted hemispheres ($H/D=0.25$) as a form factor (blue line) and comparison to the experimental data (red line).

At fig. 31 and fig. 32 the hemispheres with Height/Diameter=0.30 are presented

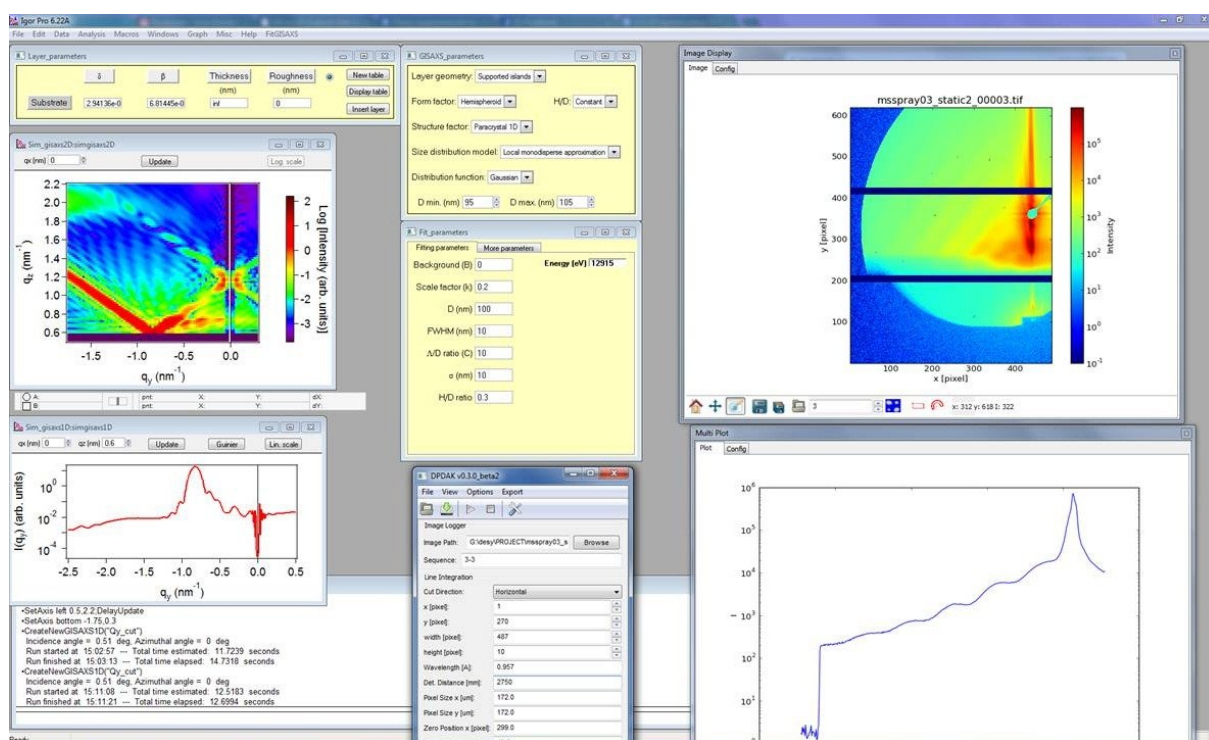


Fig.31. 2D simulated data using Tilted hemispheres (H/D=0.30) as a form factor (on the left) and comparison to the experimental data (on the right).

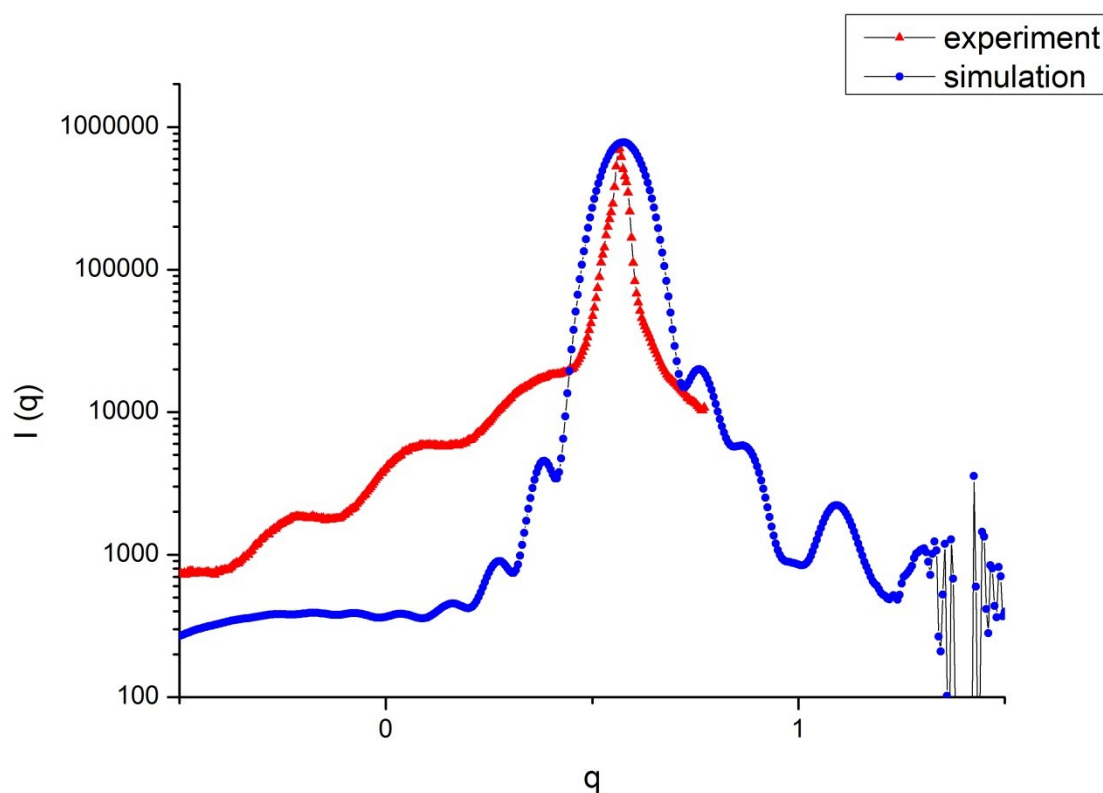


Fig.32. 1D simulated data using Tilted hemispheres (H/D=0.30) as a form factor (blue line) and comparison to the experimental data (red line).

So the best fit for the tilted hemispheres is with Height/Diameter=0.15.

At last, the **tilted cylinders** should be studied. At fig. 33 and fig. 34 they are presented

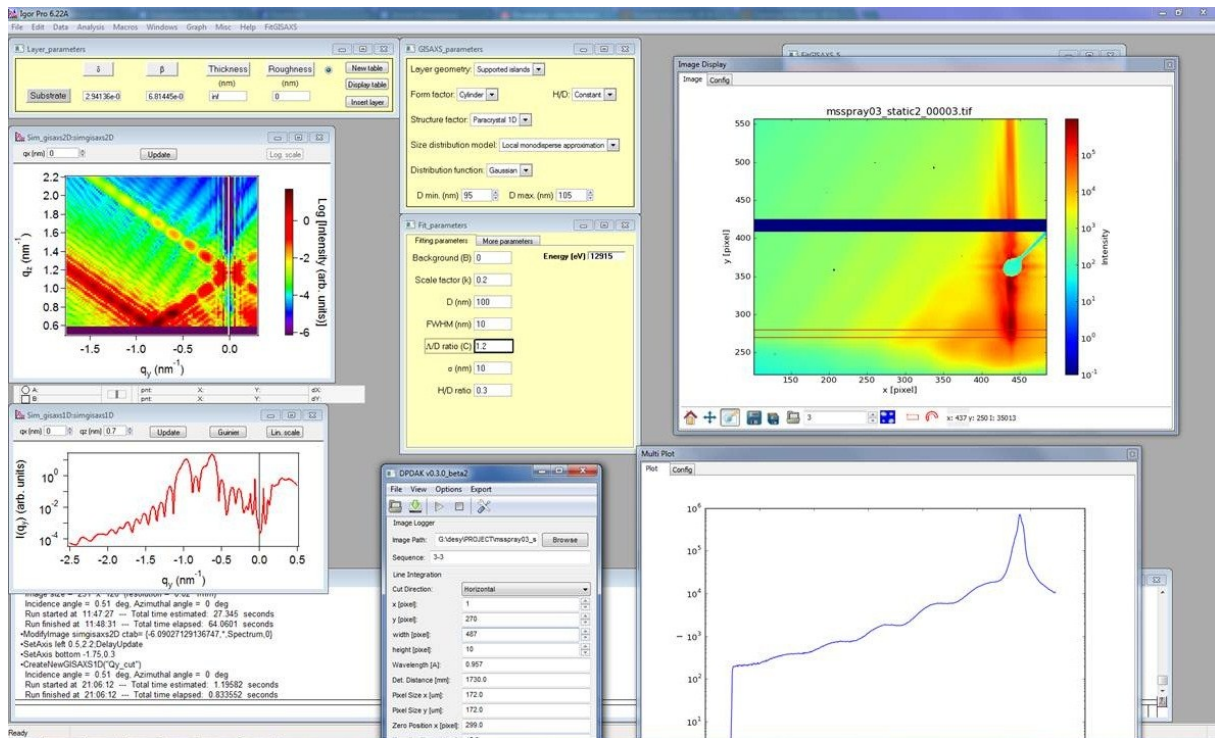


Fig.33. 2D simulated data using Tilted cylinders as a form factor (on the left) and comparison to the experimental data (on the right).

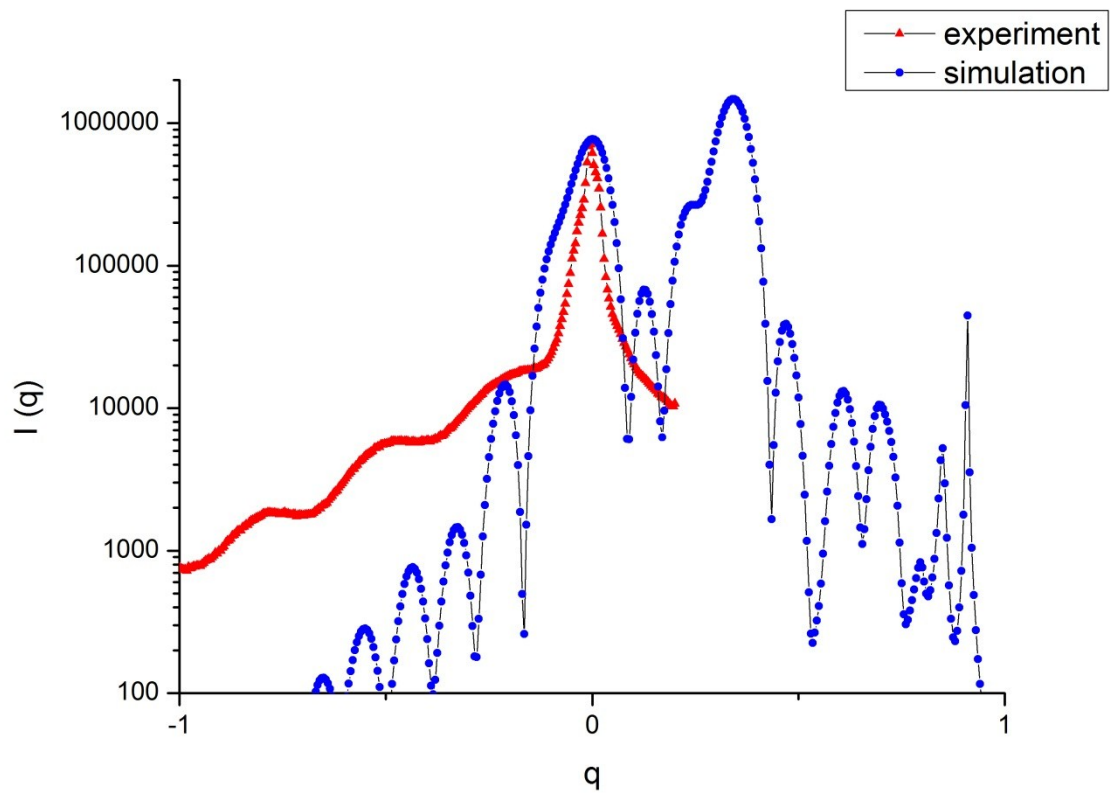


Fig.34. 1D simulated data using Tilted cylinders as a form factor (blue line) and comparison to the experimental data (red line).

To sum up, two other parameters were chosen. For the first stage the structure factor should be Paracrystal 1D and the form factor is spheroid. For the last stage the structure factor should be also Paracrystal 1D but the form factor should be tilted hemispheres or tilted cylinders. In general, the fit made with tilted hemispheres is better.

Distance

Another parameter that could be changed is the distance between particles

If the form factor as the **tilted cylinders** is used, the following results are received.

At fig.33 and fig. 34 the distance between particles is **110 nm**.

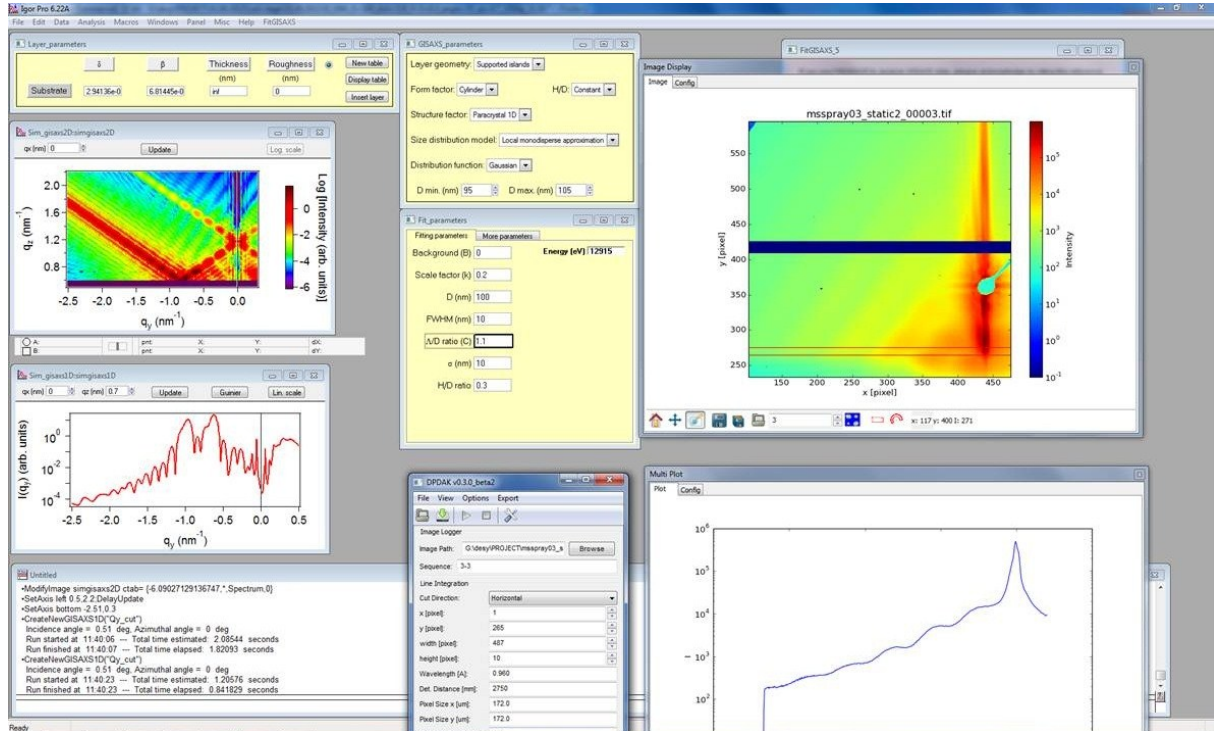


Fig.33. 2D simulated data with distance = 110 nm (on the left) and comparison to the experimental data (on the right).

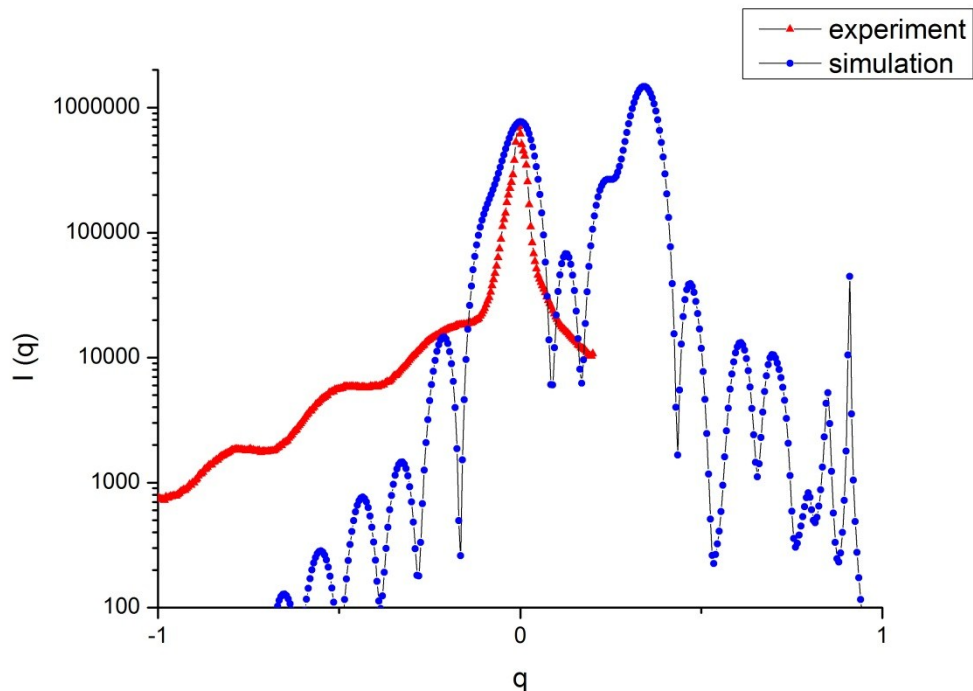


Fig.34. 1D simulated data with distance = 110 nm (blue line) and comparison to the experimental data (red line).

At fig.37 and fig. 38 the distance between particles is **130 nm**.

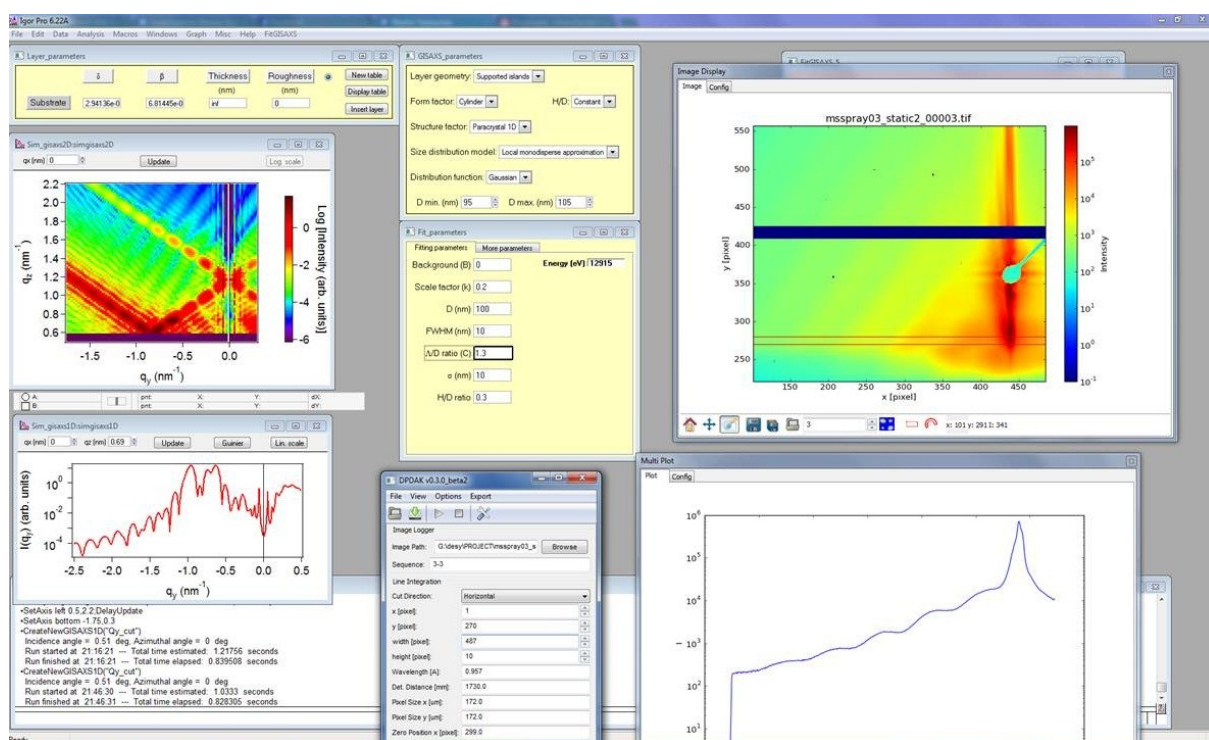


Fig.37. 2D simulated data with distance = 130 nm (on the left) and comparison to the experimental data (on the right).

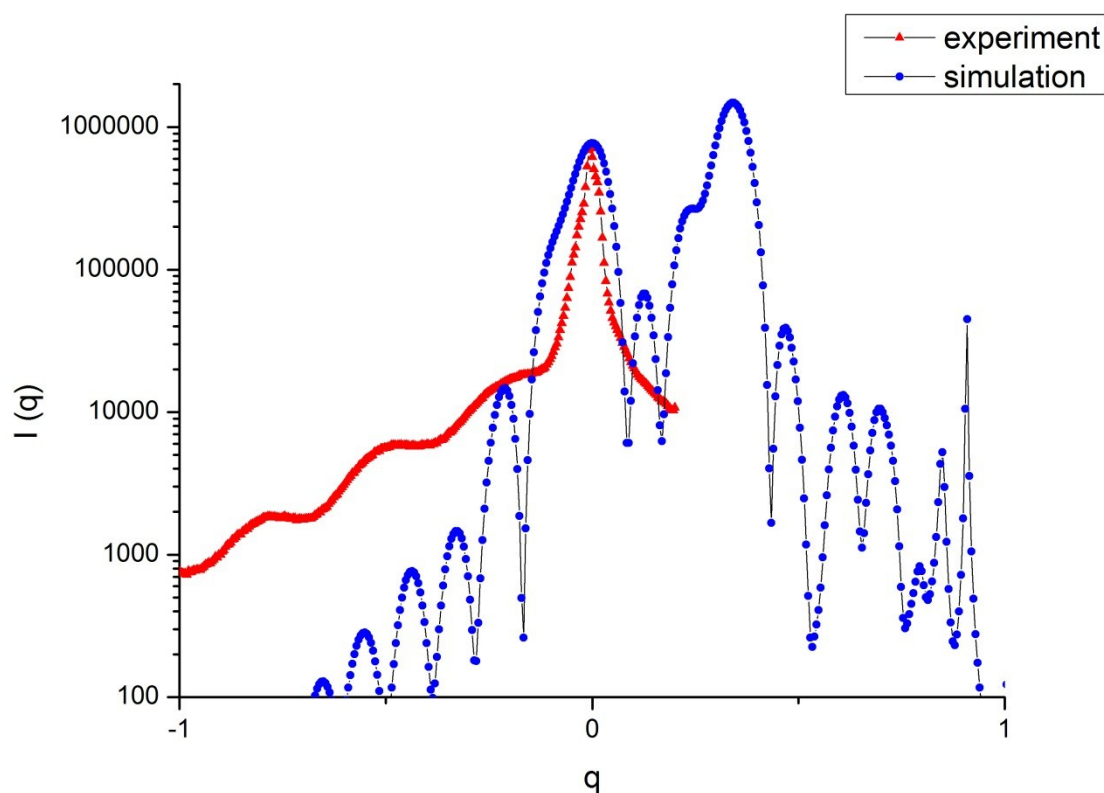


Fig.38. 1D simulated data with distance = 130 nm (blue line) and comparison to the experimental data (red line).

At fig.39 and fig. 40 the distance between particles is **1000 nm**.

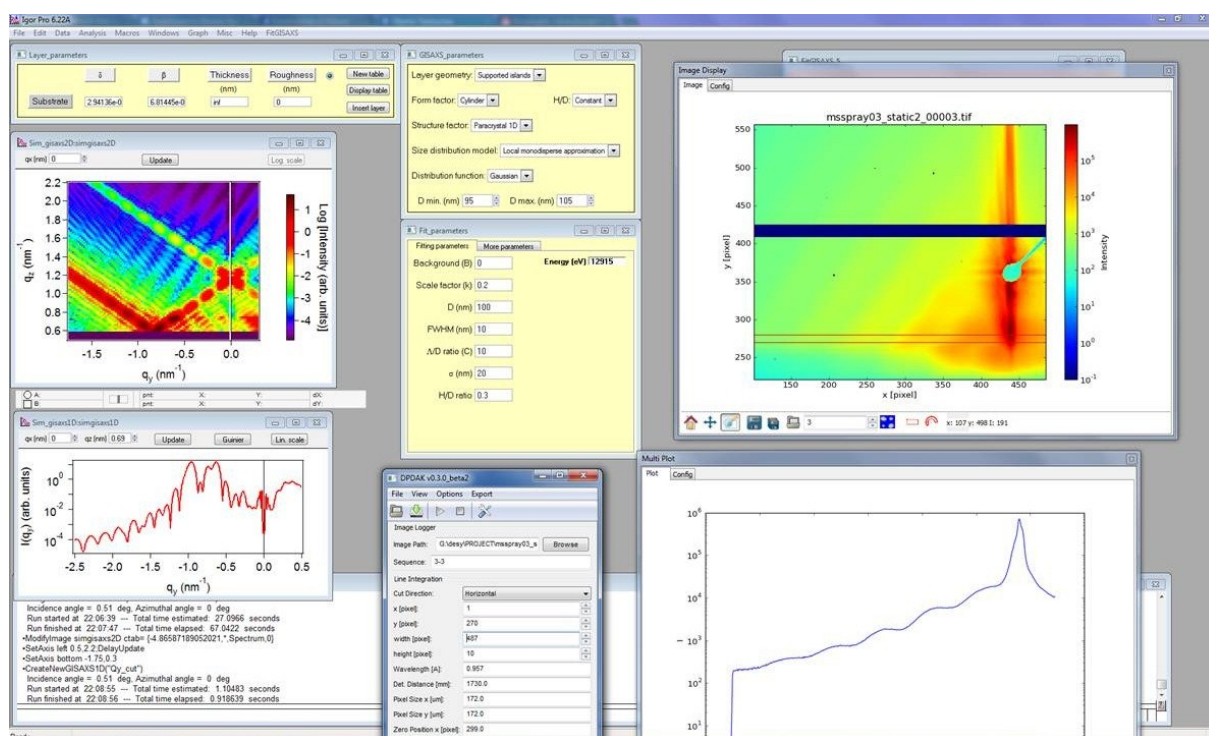


Fig.39. 2D simulated data with distance = 1000 nm (on the left) and comparison to the experimental data (on the right).

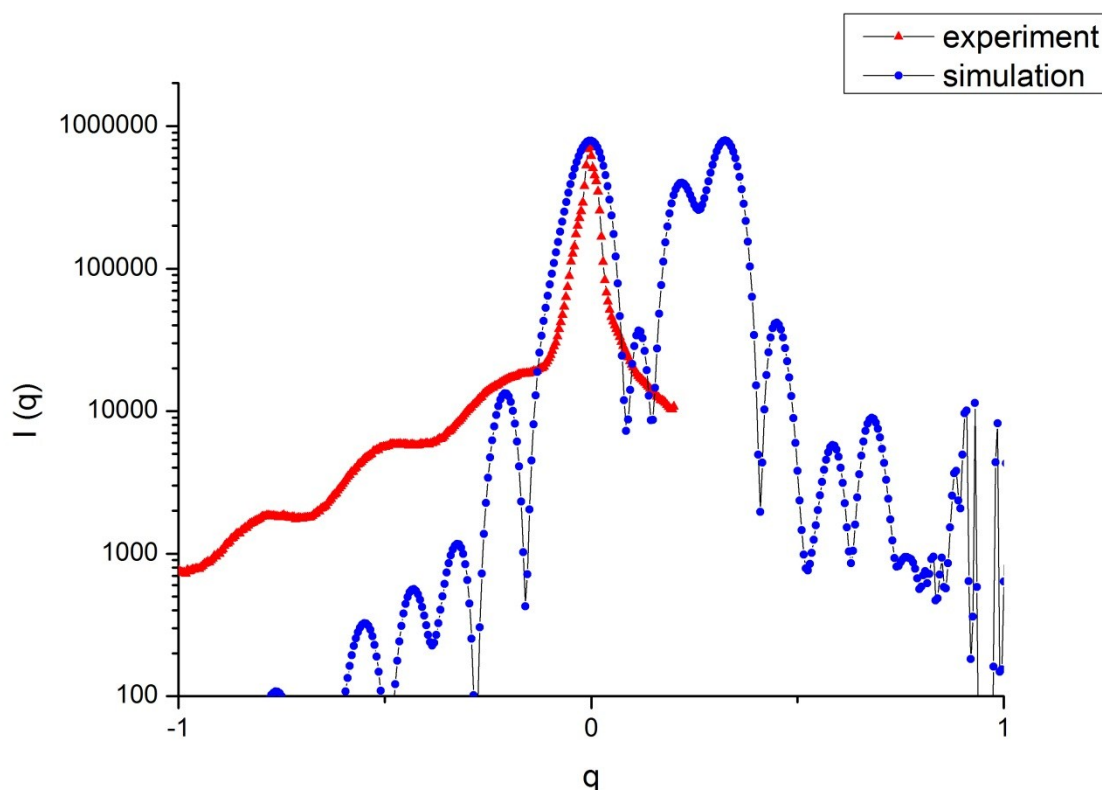


Fig.40. 1D simulated data with distance = 1000 nm (blue line) and comparison to the experimental data (red line).

So in fig. 33, 35, 37 and 39 it is clearly observed that the intense increases with the increasing of the distance. And fig. 34, 36, 38 and 40 show the better fitting of the main peak with the increasing of distance. However, the increasing of the distance till 1000nm means isolated particles on the surface that cannot be attained in reality.

If the form factor as the **tilted hemispheres** is used, the following results are received. The distance doesn't influence much when using this form factor.

At fig.41 and fig. 42 the distance between particles is **120 nm**.

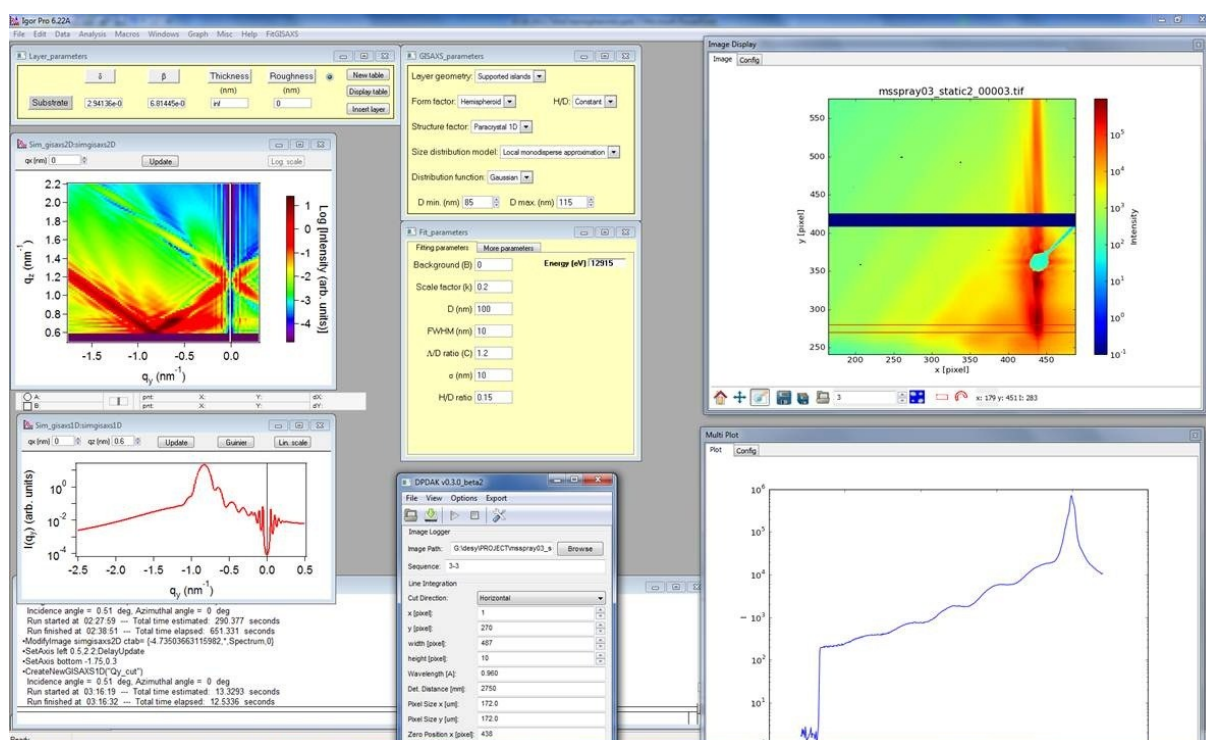


Fig.41. 2D simulated data with distance = 1000 nm (on the left) and comparison to the experimental data (on the right).

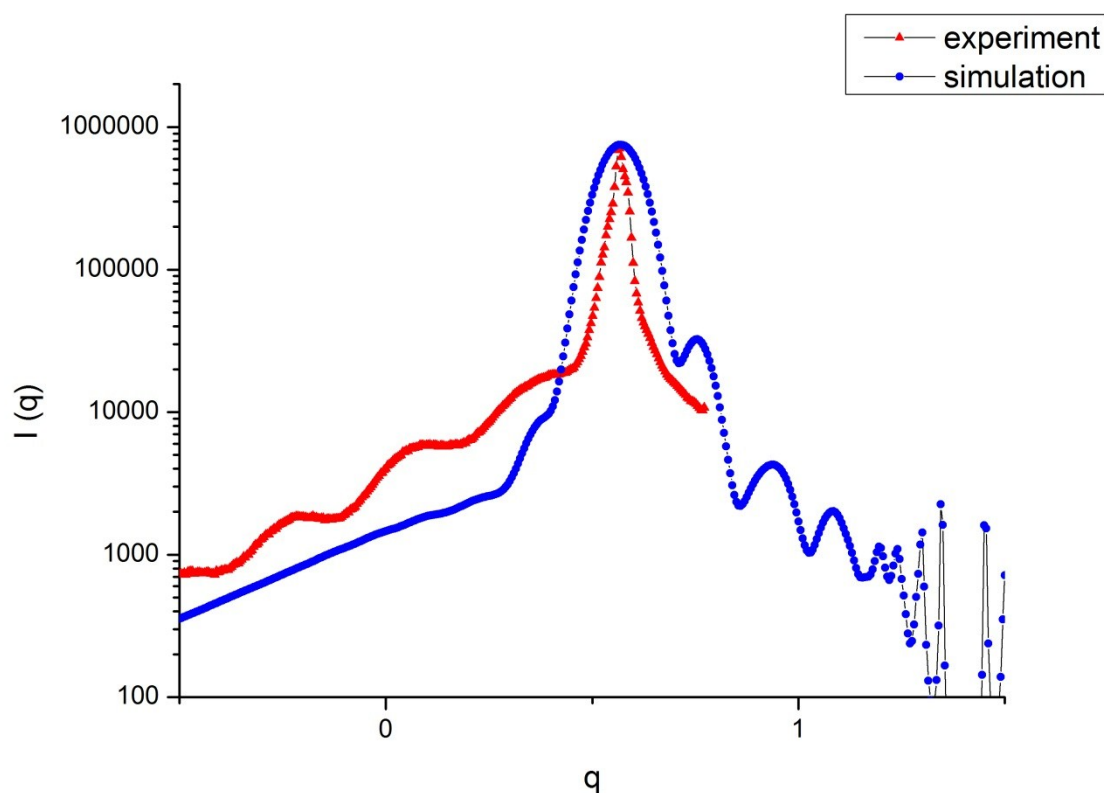


Fig.42. 1D simulated data with distance = 1000 nm (blue line) and comparison to the experimental data (red line).

At fig.43 and fig. 44 the distance between particles is **150 nm**.

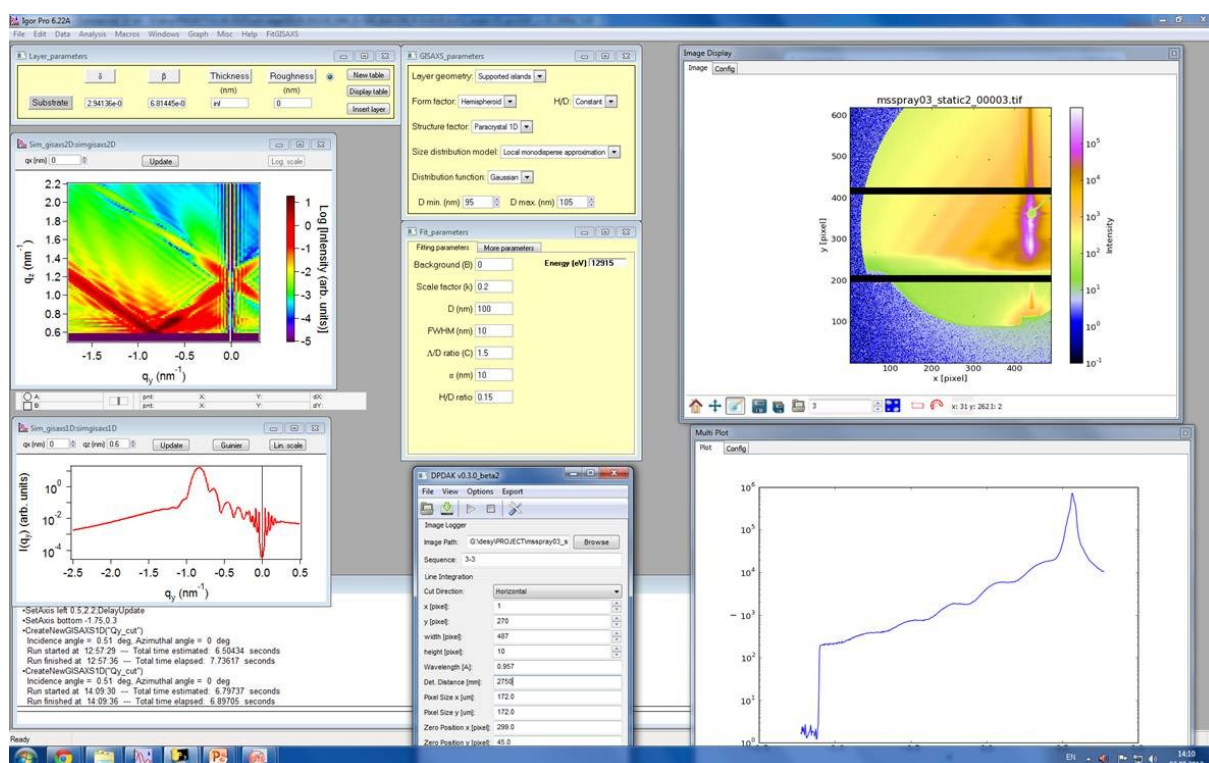


Fig.43. 2D simulated data with distance = 150 nm (on the left) and comparison to the experimental data (on the right).

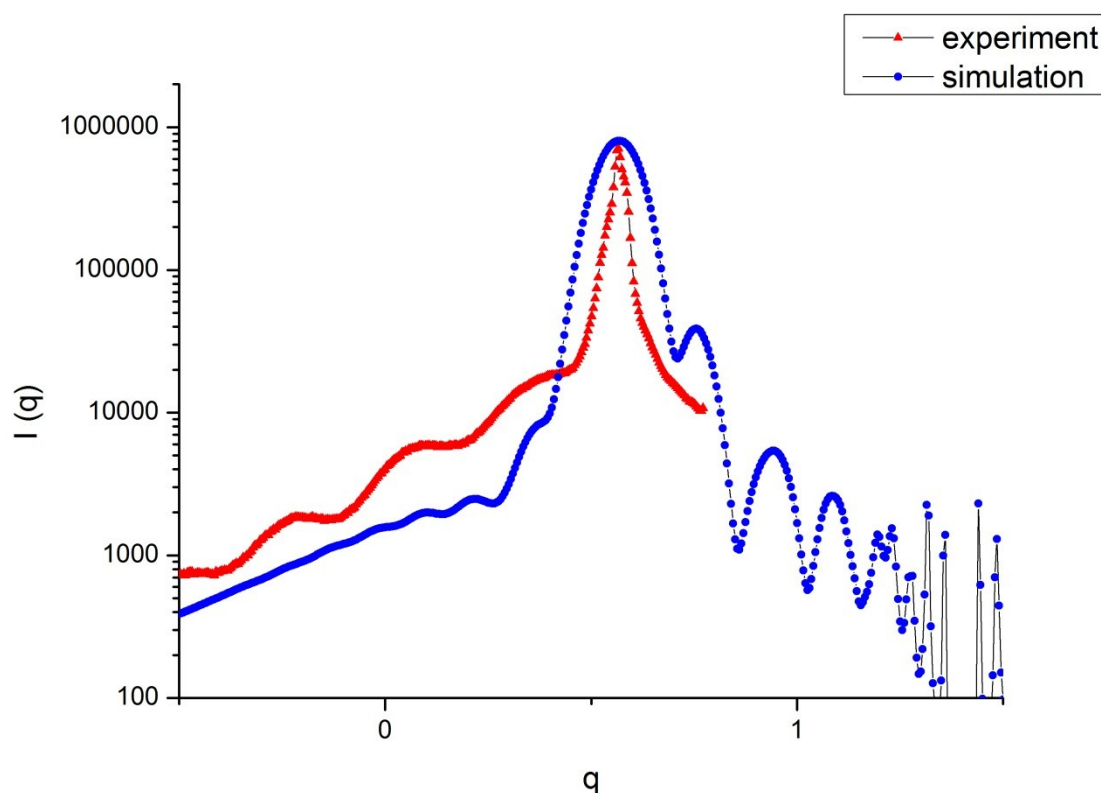


Fig.44. 1D simulated data with distance = 150 nm (blue line) and comparison to the experimental data (red line).

At fig.45 and fig. 46 the distance between particles is **1000 nm**.

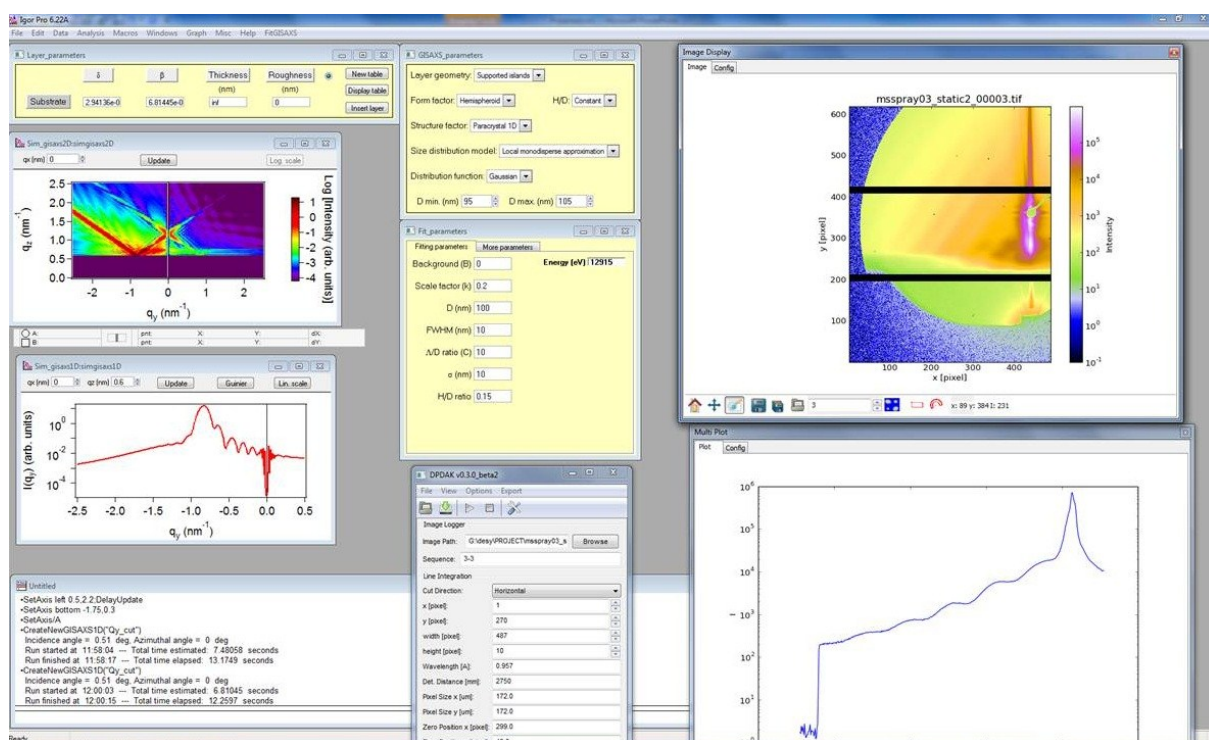


Fig.45. 2D simulated data with distance = 1000 nm (on the left) and comparison to the experimental data (on the right).

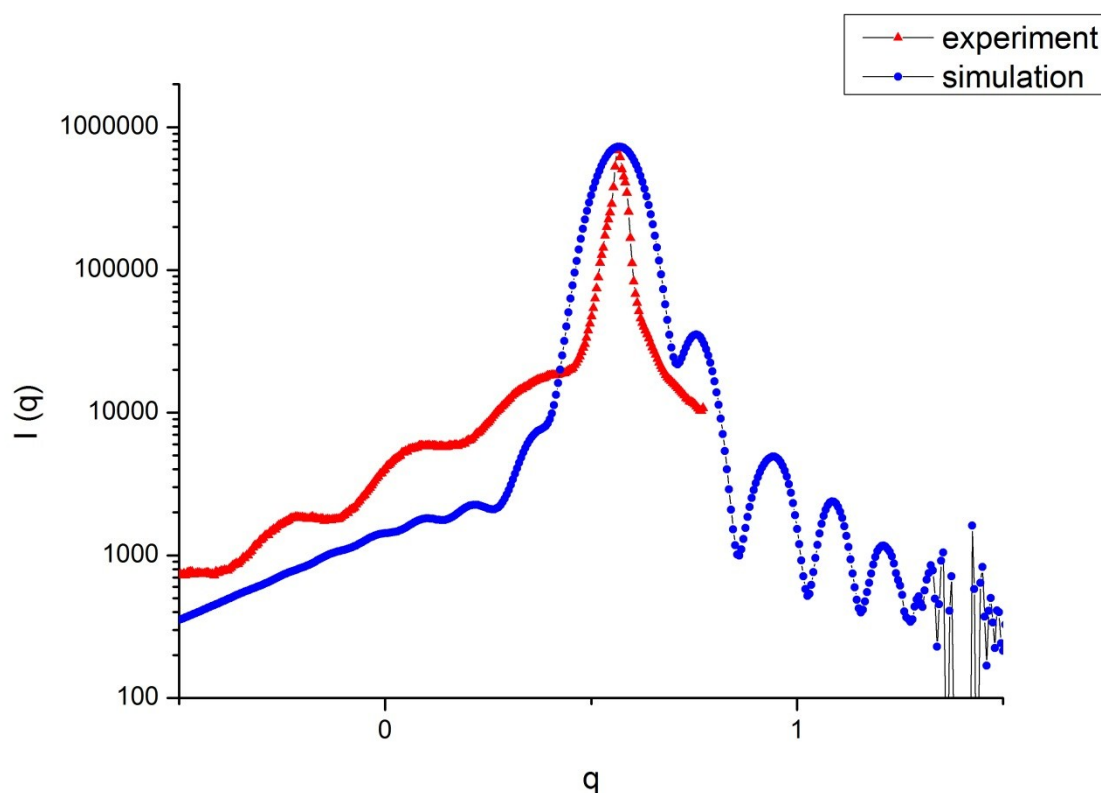


Fig.46. 1D simulated data with distance = 1000 nm (blue line) and comparison to the experimental data (red line).

Including SiO₂ layer

What else can be done to fit the experimental data is to create a new layer of SiO₂ between the substrate and PS. From chemical part, it can be better to create this layer because of the characteristics of silicon substrate.

In fig. 47 and 48 the simulations without the layer are shown.

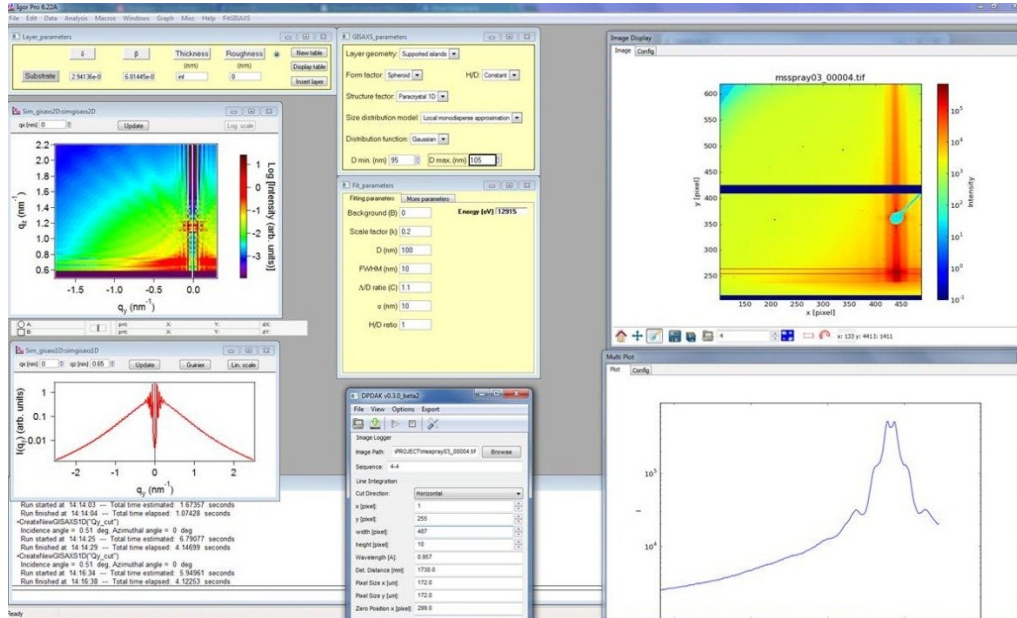


Fig.47. 2D simulated data without SiO₂ layer (on the left) and comparison to the experimental data (on the right).

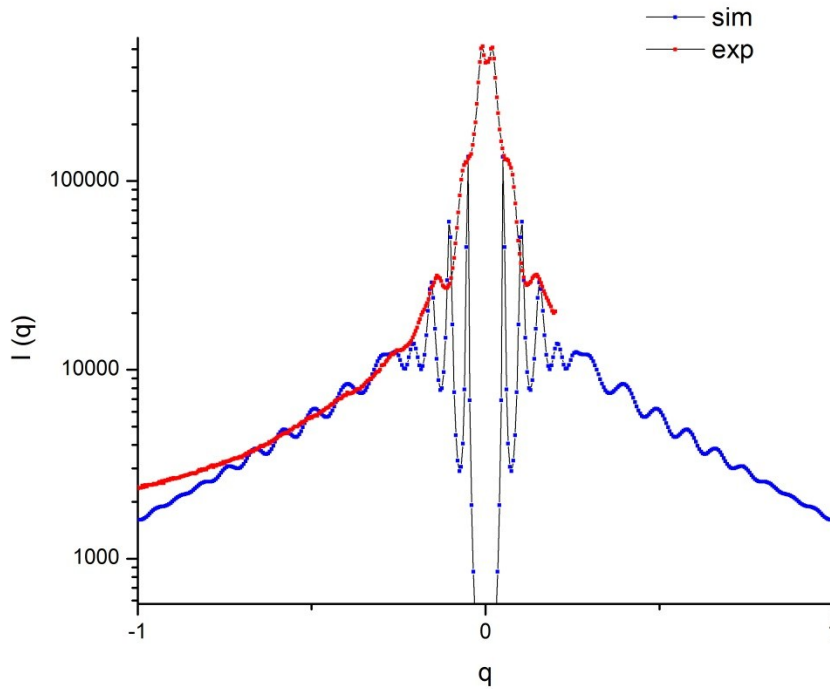


Fig.48. 1D simulated data without SiO₂ layer (blue line) and comparison to the experimental data (red line).

In fig. 49 and 50 the simulations including the layer of silicon oxide are shown.

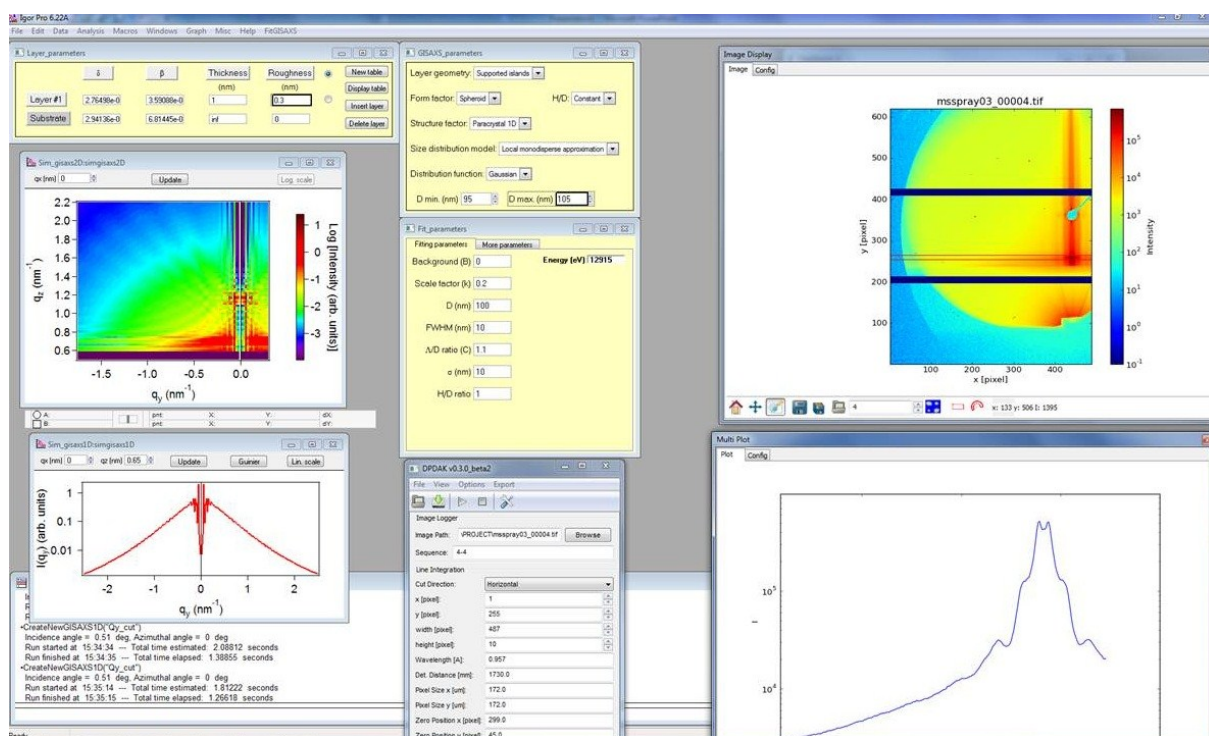


Fig.49. 2D simulated data including SiO₂ layer (on the left) and comparison to the experimental data (on the right).

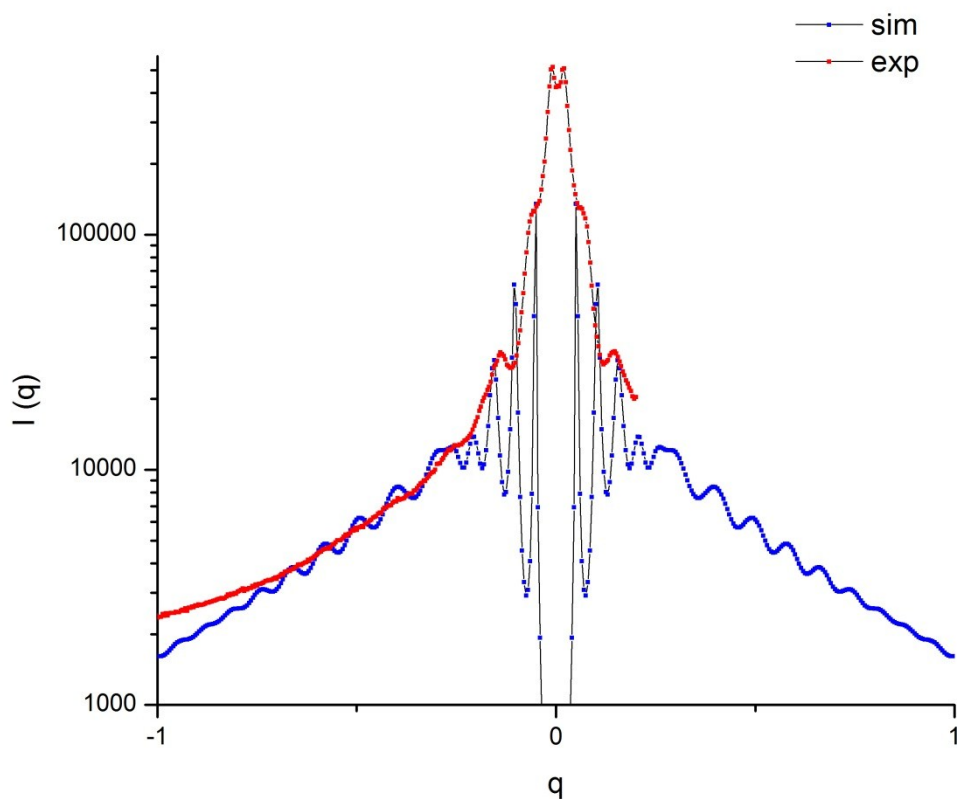


Fig.50. 1D simulated data including SiO₂ layer (blue line) and comparison to the experimental data (red line).

As it can be easily noticed, there is no visible difference between them. So we can choose any option we want in this parameter.

Conclusions

As a result of this work the following parameters were chosen to fit the experimental data.

For first stage (sample 1) the best fit is (fig.17 and 18):

Parameter	Choice
Layer geometry	Supported islands
Size distribution model	Local Monodisperse Approximation
Structure factor	Paracrystal 1D
Form factor	Spheroid
Distance	110-120 nm
Including SiO ₂ layer	any

For last stage (sample 2) the best fit is (fig.41. and 42.):

Parameter	Choice
Layer geometry	Supported islands
Size distribution model	Local Monodisperse Approximation
Structure factor	Paracrystal 1D
Tilt angle	55 degrees
Form factor	Tilted hemispheroids
Height / Diameter	0.15
Distance	120 150 nm
Including SiO ₂ layer	any

References

- [1] Müller-Buschbaum P.: *A Basic Introduction to Grazing Incidence Small-Angle X-Ray Scattering*. Lect. Notes Phys. 776, 61–89 (2009)
- [2] P.Müller-Buschbaum, E Bauer., E.Maurer, S. V.Roth, R.Gehrke, M.Burghammer, C.Riekel: *Large scale and local scale structures in polymer blend films: A GIUSAXS and sub-microbeam GISAXS investigation*; Appl. Cryst. 40, s341 (2007). 62, 63
- [3] Dr. A. Buffet, Dr. M. M. Abul Kashem, Dr. J. Perlich, G. Herzog, M. Schwartzkopf, Dr. R. Gehrke, Dr. S. V. Roth: *Stripe-Like Pattern Formation in Airbrush-Spray Deposition of Colloidal Polymer Film*, ADVENGMAT, ISSN 1438-1656, Vol. 12 – No. 12 (2010)
- [4] D. Babonneau: *FitGISAXS : software package for modelling and analysis of GISAXS data using IGOR Pro*, J. Appl. Crystallogr. 43 (2010) 929–936.
- [5] <http://www.physics.queensu.ca/~saxs/GISAXS.html>
- [6] <http://en.wikipedia.org/wiki/Paracrystalline>
- [7] Rémi Lazzari: IsGISAXS - a tool for Grazing Incidence Small Angle X-ray Scattering analysis for nanostructures (Version 2.6) (http://ln-www.insp.upmc.fr/axe4/Oxydes/IsGISAXS/figures/doc/manual.html#tth_sEc2.4.1)

Acknowledgments

I would like to thank my supervisor Stephan Roth for support, time spending and sharing the knowledge. Thanks to him I learnt a lot of new things either in GISAXS theory or in practical application in computer simulation.

Also I would like to thank I would like to thank all people who made this trip possible for me, all people of DESY for their kindness to all summer students, all of the members of FS-PE group for their willingness to help us and the good cooperation with summer students. It was great experience and unforgettable summer.

Comments

How to save the data from FitGISAXS (IgorPro6 – limited version):

It does not save any data except for table copies for 1D cuts. It can be done:

- 1) Right click → Edit simgisaxs 1D
- 2) File → Save Table copy → write the name with “.txt”

It does not let you make print screens. Open any other program (for example, DPDAK) and place pictures so everything can be seen and then make print screens and put it wherever you want.

You can't save pictures from it in demo version but you can cut them out of print screens using any other program (for example, Paint =)).

